Check for updates

ADVANCING EARTH AND SPACE SCIENCES

JGR Space Physics

RESEARCH ARTICLE
10.1029/2025JA035007

Excitation of Large Amplitude Compressional ULF Waves in the Magnetosphere by Solar Wind Pressure Spikes and IMF Southward Turning

C. Lazzeri[1], C. Forsyth[1], A. Samsonov[1], A. Fazakerley[1], M. Archer[2], T. Elsden[3], K. J. Trattner[4], J. Rae[5], and A. W. Degeling[6]

[1]Mullard Space Science Laboratory, UCL, Dorking, UK, [2]Imperial College London, London, UK, [3]University of St Andrews, St Andrews, UK, [4]University of Colorado, LASP, Boulder, CO, USA, [5]Northumbria University, Newcastle, UK, [6]School of Space Science and Technology, Shandong University, Weihai, China

Key Points:

- Large-amplitude compressional Pc5 waves are observed at geosynchronous orbit following 2 sharp pressure spikes and an Interplanetary Magnetic Field southward turning
- Drift-mirror instability driven by enhanced temperature anisotropies following the spike arrival is the most likely driver of these waves
- Ground observations reveal potential coupling of drift-mirror and shear Alfvén waves

Supporting Information:

Supporting Information may be found in the online version of this article.

Correspondence to:

C. Lazzeri,
ucaslaz@ucl.ac.uk

Citation:

Lazzeri, C., Forsyth, C., Samsonov, A., Fazakerley, A., Archer, M., Elsden, T., et al. (2026). Excitation of large amplitude compressional ULF waves in the magnetosphere by solar wind pressure spikes and IMF southward turning. *Journal of Geophysical Research: Space Physics*, *131*, e2025JA035007. https://doi.org/10.1029/2025JA035007

Received 22 DEC 2025
Accepted 9 JUL 2026

© 2026 The Author(s). Journal of Geophysical Research: Space Physics published by Wiley Periodicals LLC on behalf of American Geophysical Union. This is an open access article under the terms of the Creative Commons Attribution License, which permits use, distribution and reproduction in any medium, provided the original work is properly cited.

Abstract

We present a case study of large amplitude, compressional Pc5 waves observed by GOES 13 and 15 at geosynchronous orbit near noon. These waves were excited near the arrival time of two consecutive solar wind dynamic pressure spikes at the magnetopause, the second of which was associated with a large and rapid southward turning of the Interplanetary Magnetic Field (IMF). Magnetopause oscillations at a similar frequency were observed by the THEMIS spacecraft in the post-noon magnetosphere, however without clear signatures of compressional waves. The analysis of the ground response near the GOES foot-points, located close to the Churchill line of magnetometer stations, revealed an increase in wave power following each spike, with slight changes in polarizations. Following the second pressure spike's arrival at the magnetosphere, we found evidence of Field Line Resonances in the Northward component of the magnetic field, which suggests coupling with the compressional waves observed at GOES. We investigated potential Ultra Low Frequency drivers, and identified the most likely driving mechanism to be the drift-mirror instability; lack of appropriate measurements however prevented us from confirming this hypothesis.

Plain Language Summary

The Earth's magnetosphere is the plasma environment dominated by the planet's magnetic field. Ultra Low Frequency waves are an important part of this system, due to their role in transporting energy across its different regions and their interaction with electrons in the outer radiation belt, a region of highly energetic charged particles. Great attention has been given to understanding the driving mechanisms of these waves, which can be either external (i.e., associated with the solar wind) or internal to the magnetosphere. In this study, we present a case of ultra low frequency waves generated by consecutive spikes in the dynamic pressure exerted by the solar wind on the magnetosphere. The second spike is associated with a rapid change in the orientation of the interplanetary magnetic field. The oscillations generated by these spikes, observed by geostationary satellites orbiting near noon on the dayside magnetosphere, are parallel to the magnetic field direction and particularly large. Signatures of oscillations perpendicular to the magnetic field direction are detected with ground magnetometers. In this paper, we investigate the link between the solar wind pressure spikes, the field-aligned oscillations observed at the geostationary satellites, and the ground signatures detected by magnetometer stations.

1. Introduction

Ultra Low Frequency (ULF) waves are an essential element of magnetospheric physics; they contribute to the transport of energy across the different regions, promoting their coupling and, just as importantly, they are associated with the acceleration and loss, as well as the radial diffusion, of relativistic electrons located in the outer radiation belt (e.g., Claudepierre et al., 2013; Elkington et al., 2003; Elsden, 2025; Mann et al., 2012). ULF pulsations are commonly classified as regular (Pc) or irregular (Pi), and further divided based on their frequency; Pc1 waves are the highest frequency ULF waves, and Pc5 waves, with a period in the 150–600 s range, are at the opposite end of the ULF spectrum (Jacobs et al., 1964). The latter are of particular interest given their ability to accelerate radiation belt particles through wave-particle interactions (e.g., Elkington et al., 1999).

Within the magnetosphere, the two dominant MHD wave modes are compressional fast magnetosonic waves, which can propagate in any direction, and shear Alfvén waves, which propagate along magnetic field lines. Both of these modes can give rise to their standing counterparts, respectively known as global modes (or cavity/

21699402, 2026, 8, Downloaded from https://agupubs.onlinelibrary.wiley.com/doi/10.1029/2025JA035007 by Imperial College London, Wiley Online Library on [03/08/2026]. See the Terms and Conditions (https://onlinelibrary.wiley.com/terms-and-conditions) on Wiley Online Library for rules of use; OA articles are governed by the applicable Creative Commons License

waveguide modes) and Field Line Resonances (FLR). While global modes arise from reflection off sharp density gradients like the magnetopause or the plasmapause (Kivelson & Southwood, 1985), FLRs are generated by reflection from the highly conductive ionosphere at the two hemispheres (Chen & Hasegawa, 1974a; Southwood, 1974). Evidence of coupling between fast modes and FLRs at field lines with the corresponding resonant frequency has been regularly observed in the magnetosphere (e.g., Chen & Hasegawa, 1974b; Kivelson & Southwood, 1986).

Gaining a better understanding of the driving mechanisms of ULF waves is crucial for using them as a diagnostic tool for magnetospheric processes. The driving processes of Pc5 waves are commonly divided into external and internal drivers. External driving mechanisms originate in the solar wind and the magnetosheath, and include solar wind dynamic pressure fluctuations (e.g., Kepko et al., 2002; Stephenson & Walker, 2002) or transient pulses (e.g., Eriksson et al., 2006; Zhang et al., 2010), the Kelvin-Helmholtz (KH) instability (e.g., Bentley et al., 2018; Mann et al., 2002; Rae et al., 2005), transient magnetopause reconnection (e.g., Glasmeier et al., 1984; Le et al., 2004; Prikryl et al., 1998), and ion foreshock phenomena (e.g., Hartinger, Angelopoulos, et al., 2013; B. Wang et al., 2020). Meanwhile, internal mechanisms involve energetic particles generating ULF waves through wave-particle interactions (e.g., drift-bounce resonance (Southwood et al., 1969)) or instabilities (e.g., drift-mirror instability (Hasegawa, 1969)). These mechanisms are often associated with geomagnetically active times, such as geomagnetic storms and substorms (e.g., Hughes et al., 1978; Yang et al., 2010). Many of these external mechanisms are responsible for the generation of waves on the magnetopause surface, which in turn generate fast mode compressional waves that propagate into the inner magnetosphere. In Murphy et al., 2015, the magnetopause location was found to also affect the ULF wave power, which the authors attributed to the fact that a more compressed magnetosphere implies external wave sources will inject energy closer to the Earth. It has been suggested that the internally generated mechanisms could also create magnetopause waves when taking place in the low- and high-latitude boundary layer (Archer et al., 2021).

Wave characteristics, such as their polarisation, propagation direction, or azimuthal scale, have been used to determine their source. For instance, the wavenumber m, which is inversely proportional to their azimuthal length scale, is often used to determine whether a wave is internally or externally driven. ULF waves whose azimuthal scale is large and comparable to that of the cavity have low wavenumbers ($m < 10$) and are usually associated with external drivers (e.g., Michael et al., 2024). Internally driven waves tend to have a smaller azimuthal size and higher wavenumbers, often indicated to be >10 in the literature. However, the sources driving waves with intermediate wavenumbers ($10 < m < 20$) are not so easily distinguished, as they have been found to be both internally (Mager et al., 2019; Michael et al., 2024; Yeoman et al., 2010) and externally (Hao et al., 2014) driven.

The wave location and polarisation can also provide information regarding the source of the waves. For instance, Murphy et al., 2018 attributed compressional waves found at large L shells to predominantly external drivers, noting that the waves are often accompanied by poloidally or toroidally polarised waves in the inner magnetosphere. Conversely, the authors attributed poloidally and toroidally polarised waves at intermediate L shells to predominantly internal generation mechanisms.

A number of ULF wave events have been associated with the arrival of interplanetary shocks at the magnetopause (e.g., Hao et al., 2014; Samsonov et al., 2011; Takahashi et al., 2023; Zong et al., 2009) and IMF discontinuities triggering foreshock perturbations (e.g., C. Wang et al., 2017). In this paper, we investigate whether a solar wind discontinuity in the form of a large and rapid ST accompanied by a dynamic pressure spike can be linked to the generation of ULF waves in the dayside magnetosphere. In a previous study, Lazzeri et al., 2024 analysed these extreme southward turnings, evaluating the strength and timescales of the geomagnetic response. The authors found that these events are often shortly followed by enhanced dayside magnetopause reconnection, magnetospheric convection, and substorms, which are phenomena often directly linked to the generation of ULF waves.

2. Data

In this paper, we use a combination of data from spacecraft and ground magnetometers. Solar Wind and IMF data are provided by the ARTEMIS (Angelopoulos, 2011) P1 (i.e., THEMIS B) and P2 (i.e., THEMIS C) lunar orbiting spacecraft which were upstream of the Earth during the event of interest. The GSM magnetic field data are provided by the fluxgate magnetometer (FGM) instrument (Auster et al., 2008) at ~3 s resolution. Particle data are obtained from the Electrostatic Analyser (ESA) instrument (McFadden et al., 2008) at ~4 s resolution, except for particle velocities, which were not available in reduced-mode at the time and were therefore obtained

Table 1
Magnetic Latitude and Longitude of Ground Magnetometer Stations and of the GOES and THEMIS Foot-Points According to the TS04 and IGRF Models

Name	M. Latitude (°)	M. Longitude (°)
Gillam (GILL)	65.73	−26.06
Island Lake (ISLL)	63.23	−25.76
Little Grand Rapids (LGRR)	61.43	−26.91
Pinawa (PINA)	59.64	−27.46
Thief River Falls (THRF)	57.47	−27.73
GOES 13	66.26	−2.20
GOES 15	66.32	−16.96
THEMIS A	68.72	18.96
THEMIS D	69.20	20.30
THEMIS E	69.05	22.11

from the space moments, at ∼4 s resolution. We examined the moments data quality flags, which revealed good-quality data across the interval we considered except between ∼17:31–17:38 and after 19:00, when the electron densities were more than twice the ion densities. Similarly, we obtain the THEMIS A, D, and E data from the corresponding instruments, although at 3 s resolution. At geosynchronous orbit, GSM magnetic field data is collected by NOAA's GOES 13 and 15 (GOES N Series Data Book, 2010) FGMs at ∼0.5 s cadence. The GOES Energetic Particle Sensor–Magnetospheric Electron Detector (EPS-MAGED) provided 1-min resolution electron fluxes in 5 energy bands. Additionally, we use ground magnetometer data in NEZ coordinates and 1 s time resolution, provided by the SuperMAG collaboration (Gjerloev, 2012): we include data from the Churchill line magnetometers Gillam, Island Lake (ISLL), Little Grand Rapids (LGRR), Pinawa, and Thief River Falls. Information about these stations' magnetic coordinates are found in Table 1 and in Figure 4.

3. Southward Turning on 26 September 2011

On September 26th, 2011, the ARTEMIS P1 spacecraft was located in the solar wind at $[56.8, -10.0, -1.3]_{\mathrm{GSM}}$ R_E (Figure 1g) and observed a large and rapid ST of the IMF at 17:28 UTC (Figure 1a). Within a minute, ARTEMIS P2, located at $[52.9, -12.7, 0.2]_{\mathrm{GSM}}$ R_E, also observed the discontinuity. The turning, preceded by approximately an hour of strongly northward IMF, consisted of a ∼40 nT jump from positive to negative B_z, followed by ∼1 hr 30 min of mostly steady southward IMF. At the same time as the turning, ARTEMIS P1 observed a spike in solar wind dynamic pressure, which increased from ∼2 nPa to almost 4 nPa (Figure 1b) for ∼1 min and was driven by a brief density enhancement (density data are shown in Figure S1 in Supporting Information S1). Additionally, the solar wind speed increased by approximately 5%, from ∼530 km s^{-1} before the event to 570 km s^{-1} afterwards (Figure 1c). On this date, Richardson & Cane, 2024 reports a storm sudden commencement, potentially associated with the arrival of an ICME shock at Earth, at 12:34 UTC, and estimated the ICME leading edge arrival to be around 20:00 UTC; the observed solar wind conditions were likely within an ICME sheath. Using an average solar wind velocity of 530 km s^{-1} and propagation from ARTEMIS-P1 to the average bow shock nose distance (taken to be ∼15 R_E (Fairfield, 1971)), plus a magnetosheath propagation time of ∼16 min (Samsonov et al., 2018) gives an arrival time at the magnetopause of 17:37.

Five spacecraft were located in the dayside magnetosphere at the time of the ST (Figure 1h). The two geosynchronous spacecraft GOES 13 and 15 were located near the subsolar magnetopause, within approximately one hour of local time from each other. Further out, were THEMIS A, D, and E, (from now on referred to as THA, THD, and THE) located in the post-noon magnetosphere at approximately 14 hr MLT. THD and THE were located at similar radial distances, slightly closer to the expected equilibrium magnetopause than THA at the beginning of the event. The THEMIS magnetic field data reveals field reversals in the GSM B_z components between 17:57 and 18:08, with three reversals for both THD and THE (Figure 1d). Brief field reversals are observed again between 18:22 and 18:26, during a temporary drop in solar wind dynamic pressure. As we show in detail in Section 4.4, these reversals are signatures of magnetopause crossings, hence the THEMIS spacecraft were located within the magnetosphere at the time of the ST arrival, and crossed the magnetopause shortly after. The multiple magnetopause crossings in THD and THE suggest that the magnetopause was oscillating during our event. Near the arrival time of the ST at the magnetopause, at 17:37, GOES 13 observed oscillations predominantly in the B_z component (Figure 1e). The GOES 13 B_z oscillations show a large increase in wave power from ∼17:50, at which point similar oscillations were observed by GOES 15, approximately 2 R_E dawnward of GOES 13. The waves showed a gradual damping of the wave amplitude until 18:40, when the amplitude of B_z oscillations of both spacecraft was observed to grow again.

Before the arrival of the ST, the SYM-H and PCN geomagnetic indices show enhanced yet decaying geomagnetic activity (Figure 1f), as expected after a period of strongly northward IMF in an ICME sheath. SYM-H, driven below the −50 nT storm threshold by a previous period of southward IMF between approximately 15:30 and 16:30, begins slowly increasing from 17:00. Near the ST arrival, at 17:38, it increases sharply by 10 nT, and then

21699402, 2026, 8, Downloaded from https://agupubs.onlinelibrary.wiley.com/doi/10.1029/2025JA035007 by Imperial College London, Wiley Online Library on [03/08/2026]. See the Terms and Conditions (https://onlinelibrary.wiley.com/terms-and-conditions) on Wiley Online Library for rules of use; OA articles are governed by the applicable Creative Commons License

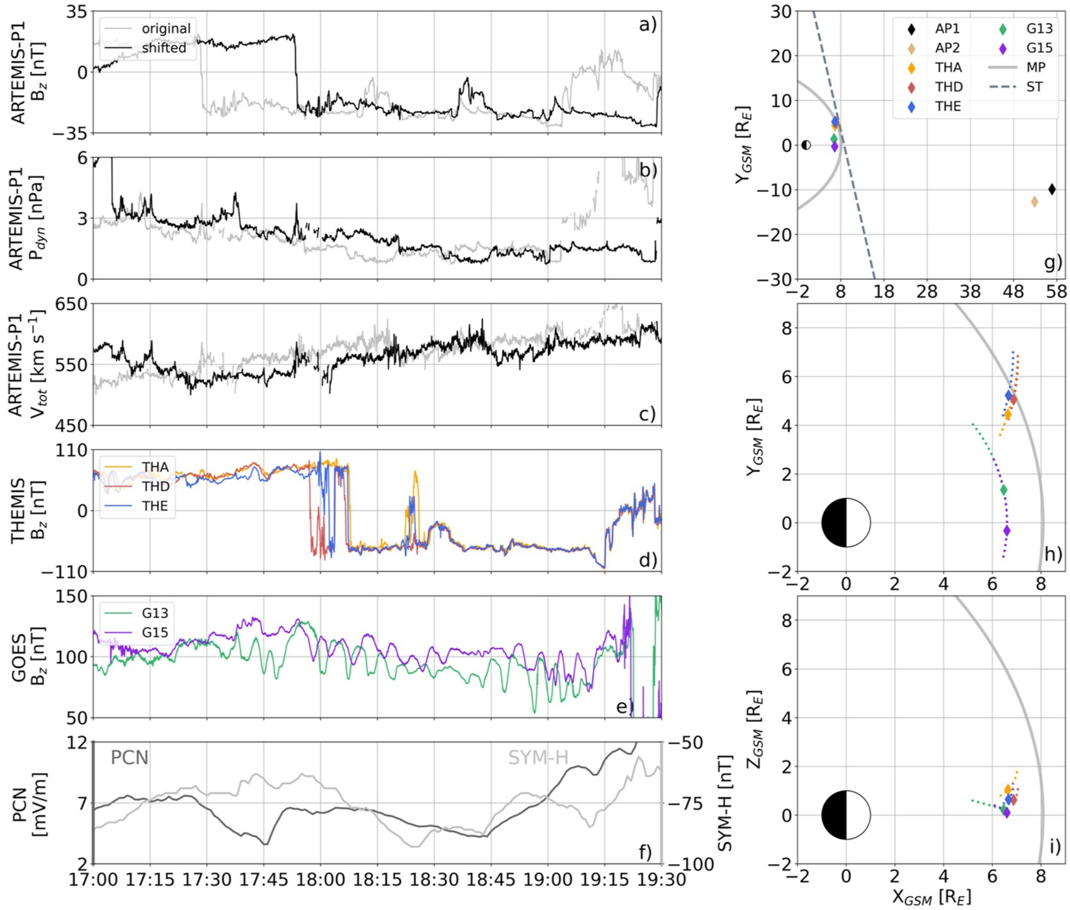

Figure 1. Event on September 26th, 2011. (a–c) Interplanetary Magnetic Field B_z, solar wind P_{dyn} and speed observed by ARTEMIS-P1 (original and shifted by 25 min), (d, e) GSM B_z components measured by the THEMIS and GOES spacecraft, respectively, (f) Geomagnetic indices PCN and SYM-H, (g–i) projections of the magnetopause and spacecraft locations in the XY and XZ GSM planes. The southward turning orientation is indicated by the gray dashed line in (g). The shape of the magnetopause in this Figure (gray solid line) is derived from the Shue et al., 1998 model for $B_z = -20$ nT and $P_{dyn} = 3$ nPa, but has been moved forward by 0.5 R_E to approximately intersect the THEMIS orbit at the location of the magnetopause crossings.

gradually decreases until ∼18:25, where, despite the strongly southward IMF, it begins gradually increasing again. Meanwhile, the PCN index, also enhanced by the previous driving, starts rapidly decaying at 17:27, before reaching a minimum at 17:45 and starting to increase again.

4. Analysis and Results

4.1. Characterisation of Magnetospheric Pc5 Waves

In order to characterise the wave observed by GOES, we convert the magnetic field data from GSM into field-aligned coordinates. For each spacecraft, we obtain the field aligned direction, **F** by normalising the mean, low-pass filtered (with a 30 min cut-off) magnetic field vector. We calculate the azimuthal direction, **A** from the cross product between **F** and the normalised mean spacecraft position vector, and the radial direction, **R**, from **A** × **F**. The transformed data is shown in Figure 2a–2c.

The data in field-aligned coordinates shows that the oscillations are largest in the field-aligned (compressional) component (Figure 2a), although they are also present in the azimuthal (toroidal) and radial (poloidal) components (Figures 2b and 2c). We note that the G13 azimuthal and radial component oscillations become clearer after the wave amplitude enhancement in B_f at 17:53.

21699402, 2026, 8, Downloaded from https://agupubs.onlinelibrary.wiley.com/doi/10.1029/2025JA035007 by Imperial College London, Wiley Online Library on [03/08/2026]. See the Terms and Conditions (https://onlinelibrary.wiley.com/terms-and-conditions) on Wiley Online Library for rules of use; OA articles are governed by the applicable Creative Commons License

21699402, 2026, 8, Downloaded from https://agupubs.onlinelibrary.wiley.com/doi/10.1029/2025JA035007 by Imperial College London, Wiley Online Library on [03/08/2026]. See the Terms and Conditions (https://onlinelibrary.wiley.com/terms-and-conditions) on Wiley Online Library for rules of use; OA articles are governed by the applicable Creative Commons License

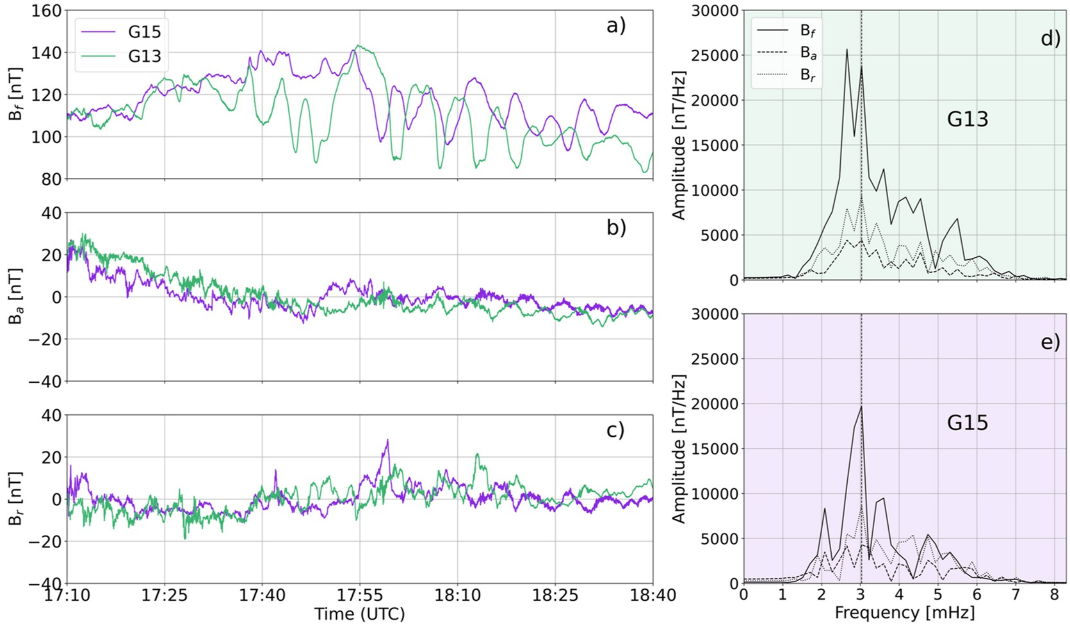

Figure 2. (a–c) GOES high-resolution magnetic field data in field aligned coordinates (from top to bottom: field-aligned, azimuthal, radial) for GOES 13 (green) and GOES 15 (purple), (d, e) FFTs of the magnetic field components of GOES 13 (green) and GOES 15 (purple). The vertical dashed line in (d, e) indicates the 3.03 mHz frequency.

We apply a 2–6 mHz bandpass filter to the GOES magnetic field data between 17:10 and 18:40 and we then apply a Fast Fourier Transform (FFT) to each component to determine the frequency of the observed oscillations. Our results are shown in Figures 2d and 2e. The FFTs of all magnetic field components in both G13 and G15 present a maximum at 3.03 mHz, although with different amplitudes. The G13 B_f FFT also has a peak at 2.65 mHz, which is slightly higher than the peak at 3.03 mHz. The obtained 3.03 mHz frequency allows us to classify the observation as a PC5 type ULF wave (Jacobs et al., 1964).

4.1.1. Propagation Direction, Velocity, and Azimuthal Wave Number

Additional information on the ULF wave, such as its propagation direction and velocity and its azimuthal scale, can be used to derive information on the wave sources (e.g., Murphy et al., 2018; Takahashi et al., 1985). The presence of two GOES spacecraft at geosynchronous orbit, with azimuthal separation of 14.6°, can help us determine such characteristics.

Firstly, we assume the propagation direction to be westward, as the oscillations are first observed in G13 and then in G15. As G13 is slightly more tailward (by 0.1 R_E) than G15, this would seem to imply that the disturbance travels sunward and is therefore not typical of externally driven waves; however, as discussed in Section 4.2, due to the orientation of the ST we could expect it to first hit the magnetosphere slightly towards dusk. Hence, westward propagation would be compatible with external wind driving if the spacecraft were located dawnward of the region where the drivers impacted on the magnetopause. Archer et al., 2021 also demonstrated that externally driven surface eigenmodes would propagate towards the subsolar point (i.e., westward on the duskside) as stationary waves, when impulsively excited within approximately 3 hr of noon. We cross-correlated the waveforms between 17:10 and 18:40 to determine the lag between them, although this is made difficult by the periodic nature of the signals. The largest peaks in correlation suggested a lag of either 2.3 or 8.2 min, giving propagation velocities of 78 km s^{-1} and 22 km $^{-1}$, respectively, which in turn correspond to azimuthal wave numbers of −10.3 and −36.8 (from $m = \frac{2\pi R_E L f}{v_{ph}}$ where f is the wave's frequency, v_{ph} is its phase velocity, m the azimuthal wave number, and L indicates the L-shell (Takahashi et al., 1985)).

The azimuthal wave number m can also be determined from the cross phase of the oscillations between the two spacecraft, which we obtain from the field-aligned component of the magnetic field. At the 3.03 mHz frequency, we find good coherence (0.94) and a cross phase of −132.6°, which, divided by the azimuthal separation of the

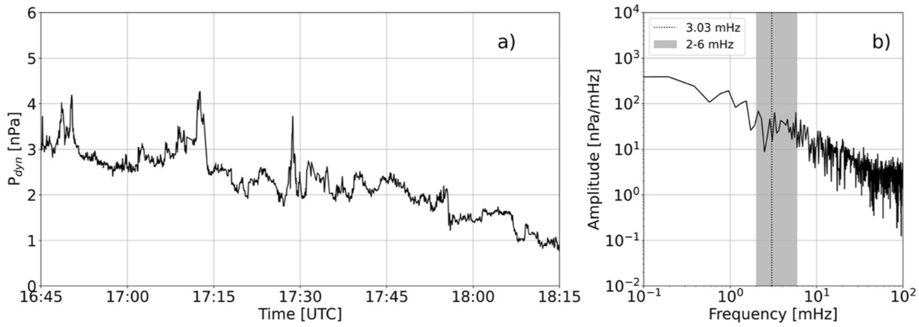

Figure 3. ARTEMIS P1 solar wind dynamic pressure (a) and its corresponding Fast Fourier Transform (b).

spacecraft (14.6°), yields an azimuthal wave number of −9.1. However, this method is subject to a $2n\pi$ ambiguity, meaning that the wave number could be higher (e.g., −33.7, −58.4, etc.). Both methods are consistent, but cannot unambiguously reveal the wavenumber.

The azimuthal wavenumber affects the observation of waves from the ground, with large-*m* waves being attenuated by ionospheric and atmospheric screening (Hughes & Southwood, 1976). However, if the *m*-number of the observed waves was to be ∼35, the wave would likely not be fully screened (e.g., Claudepierre et al., 2013).

4.2. ARTEMIS P1 Data Analysis

We analyse the solar wind and IMF data provided by ARTEMIS-P1 to investigate a potential link between the solar wind conditions and the ULF waves observed by GOES.

Firstly, we examine the fluctuations in ARTEMIS-P1 solar wind dynamic pressure. We apply a FFT to the data between 16:45 and 18:15, shifting the interval used for Figure 2 by 25 min to account for solar wind propagation, to determine whether significant oscillations in the Pc5 range were observed. The results are shown in Figure 3. We notice that the dynamic pressure spectrum resembles a power law, and does not display significant power in the Pc5 range. We repeat the same process for IMF B_z between 17:34 and 18:10 (not shown), and find no significant power in the Pc5 range.

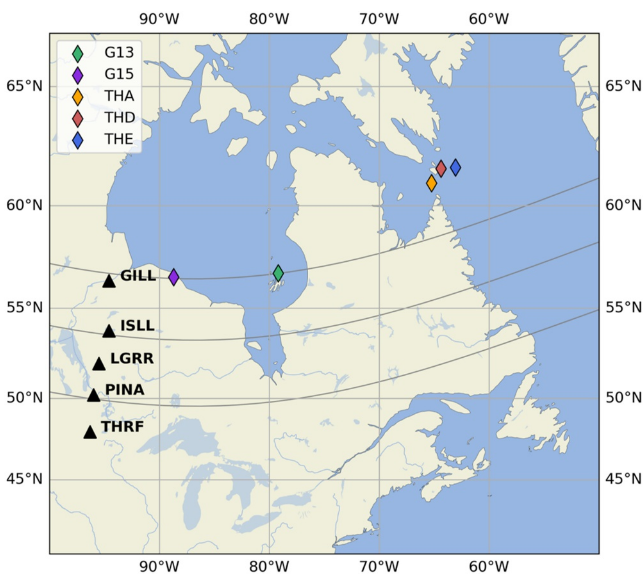

Figure 4. Map displaying the locations of ground magnetometer stations used in this study, and the footprints of the GOES and THEMIS spacecraft, as predicted by the Tsyganenko TS04 model. The gray lines indicate lines of constant magnetic latitude (66.3°, 63.2° and 59.6° from top to bottom).

Additionally, we use ARTEMIS P1 IMF observations to determine the orientation of the ST. Applying Minimum Variance Analysis (MVA) Sonnerup & Cahill, 1967; Paschmann & Daly, 1998 to the ARTEMIS-P1 magnetometer data between 17:24 and 17:31 yields a discontinuity normal of $[-0.90, -0.34, 0.26]_{GSM}$ (intermediate to medium Eigenvalue ratio ∼3.8). Applying the same procedure to ARTEMIS-P2 data between 17:25 and 17:32 yields a discontinuity normal of $[-0.87, -0.42, 0.25]_{GSM}$ (intermediate to medium Eigenvalue ratio ∼3.4), which is within 5° of the ARTEMIS-P1-derived normal. We show the ST orientation in Figure 1g, by the gray dashed line. Assuming that the discontinuity maintained its orientation while propagating in the solar wind and the magnetosheath, it would have first hit the magnetopause in the post-noon region.

4.3. Ground Magnetometer Observations

Field-line tracing using the Tsyganenko TS04 (Tsyganenko & Sitnov, 2005) and IGRF (Alken et al., 2021) models suggests that the GOES and THEMIS footpoints were located in Eastern Canada at the time of the event. Their exact locations are reported in Table 1 and shown in Figure 4. Here, we find several ground magnetometer stations which observe Pc5 oscillations. The Churchill line magnetometers (see Figure 5 (left panel)) observed oscillations in all components, however they were most pronounced in the northward component, B_N. The FFT of this component, filtered between 2 and 6 mHz, is also shown in Figure 5 (right panel); we note that the obtained spectra for the more northward

21699402, 2026, 8, Downloaded from https://agupubs.onlinelibrary.wiley.com/doi/10.1029/2025JA035007 by Imperial College London, Wiley Online Library on [03/08/2026]. See the Terms and Conditions (https://onlinelibrary.wiley.com/terms-and-conditions) on Wiley Online Library for rules of use; OA articles are governed by the applicable Creative Commons License

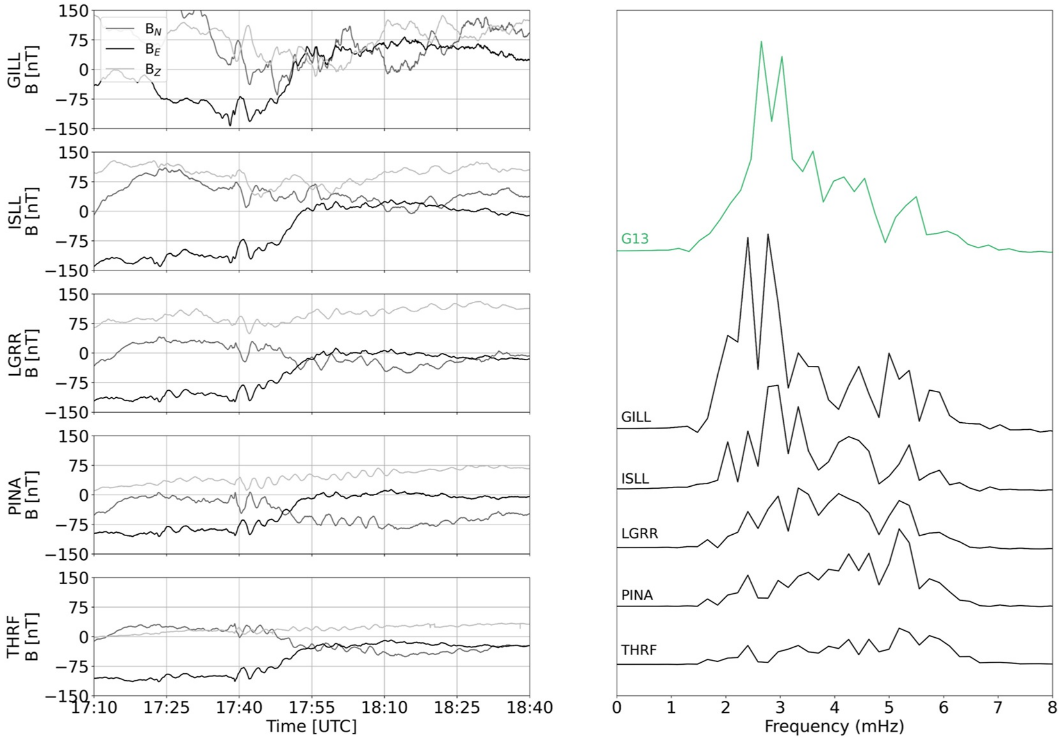

Figure 5. On the left, magnetic field data from Churchill line magnetometers in NEZ coordinates. On the right, FFTs of the G13 B_f and magnetometers' B_N components between 17:10 and 18:40.

magnetometer stations present a close resemblance to the spectrum of the G13 B_f in the same time interval, however with a slight shift to lower frequencies.

By band-pass filtering the ground magnetic field data between 2 and 6 mHz, computing the Hilbert transform, and combining them in quadrature, we obtain analytic signals and calculate their power. The filtered ground data and the corresponding power in the 2–6 mHz range are shown in Figure 6. At ∼17:39 all 5 ground magnetometers observed a sudden increase in oscillation amplitude in both B_E and B_N, in concert with the enhancement in wave activity at G13. Shortly after this, at ∼17:53, the magnetometers observed another enhancement in wave power, most significant in the B_N component. This second increase in power appeared near the beginning of wave activity at G15. The magnetic mapping of G13 and G15 to the ground suggests that G15 was magnetically closer to the Churchill line, however the observations of the wave activity seen at the ground share greater similarities to that seen by G13. We believe this may be due to incorrect field line tracing, as, as shown in Figure 7, the TS04 model does not correctly reproduce the magnetic field observations of G15. In particular, the positive offset in the modeled B_y component may have introduced a duskward shift in the longitudinal coordinate of spacecraft's footpoints, causing the G15 trace to appear between that of G13 and the Churchill line.

Hodograms of B_E against B_N for all magnetometers, separating data near the first (17:35–17:45) and second (17:45–17:55) wave power enhancements are shown in Figure 6 (right column). The hodograms show a shift in polarisation with the second increase in wave power; at ISLL and LGRR, the waves become more linearly polarised, and, across all magnetometers, the polarisation displays a slight change in direction.

To determine the presence of FLRs and obtain their frequency, we apply the cross phase method detailed in Waters et al., 1991, which requires the use of magnetic field data from magnetometer stations located at similar longitudinal coordinates but varying latitudes. We use magnetometer data between 17:50 and 18:15 and, before applying the cross phase method, we apply a 1–8 mHz band pass filter. This filtering range, larger than the 2–6 mHz previously used for GOES data, was chosen to account for variations in field line resonant frequency with magnetometer latitude. We then FFT the B_N component of each station, and calculate the amplitude and phase differences for each pair of consecutive stations by subtracting the amplitude (or phase) of the equatorward

21699402, 2026, 8, Downloaded from https://agupubs.onlinelibrary.wiley.com/doi/10.1029/2025JA035007 by Imperial College London, Wiley Online Library on [03/08/2026]. See the Terms and Conditions (https://onlinelibrary.wiley.com/terms-and-conditions) on Wiley Online Library for rules of use; OA articles are governed by the applicable Creative Commons License

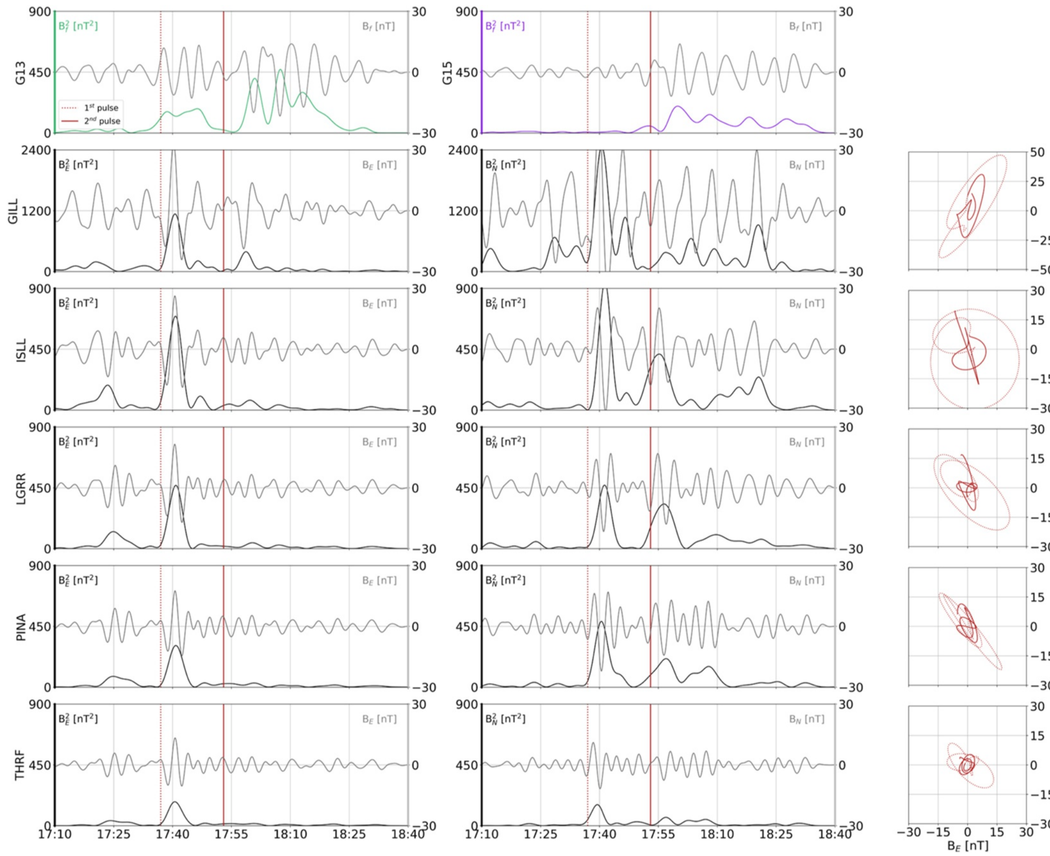

Figure 6. In the top row, the filtered B_f (gray) and the corresponding wave power for the G13 and G15 spacecraft. Below them, the same data is shown for the Churchill line magnetometers, for the B_E (left column) and B_N (middle column) components. The vertical red lines indicate the first (dotted) and second (solid) wave power enhancements. On the column on the right, hodograms of B_E versus B_N for each magnetometer and for each enhancement. Note that the *y*-axis limits for the Gillam station (second row) are different.

station from that of the poleward station. With this method, the resonant frequency would appear where the amplitude difference plotted against frequency reaches zero with a negative slope, and the cross phase displays a minimum. Our results are displayed in Figure 8. For all four consecutive pairs of stations, the amplitude difference

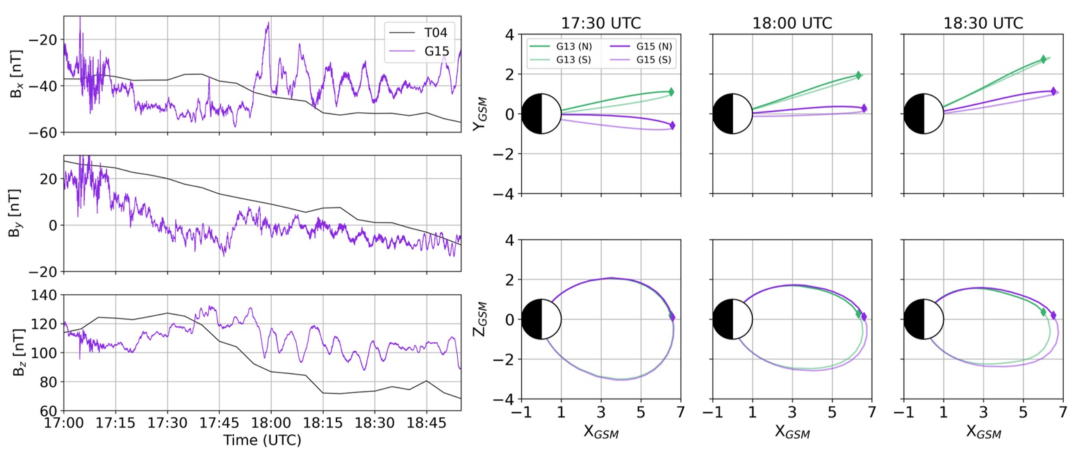

Figure 7. On the left, the comparison of G15 magnetic field data with the TS04 output along the spacecraft's orbit, both in GSM coordinates. On the right, the TS04 field line tracing for G13 and G15 at different locations along their orbit.

21699402, 2026, 8, Downloaded from https://agupubs.onlinelibrary.wiley.com/doi/10.1029/2025JA035007 by Imperial College London, Wiley Online Library on [03/08/2026]. See the Terms and Conditions (https://onlinelibrary.wiley.com/terms-and-conditions) on Wiley Online Library for rules of use; OA articles are governed by the applicable Creative Commons License

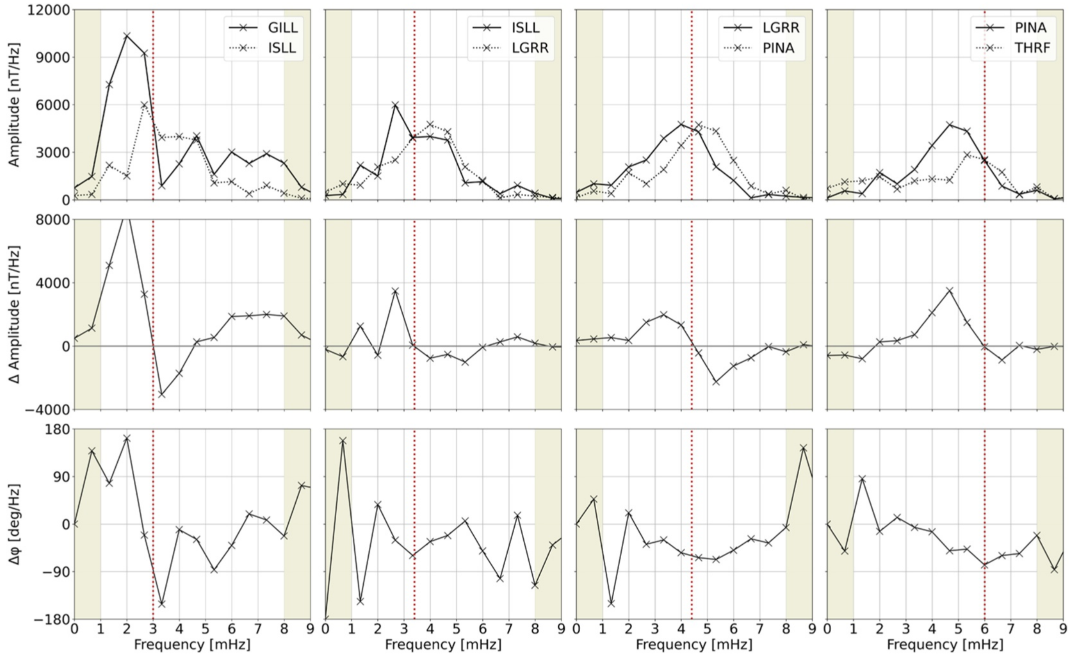

Figure 8. Test for Field Line Resonances (FLR) using pairs of Churchill Line magnetometers. The top row shows the Fast Fourier Transform of the B_N component, the middle row and bottom row show the amplitude and phase differences, respectively. The dashed line indicates the frequency of the FLR (respectively 3, 3.4, 4.4, and 6 mHz).

crosses 0 approximately near a local minimum in cross phase, which indicates the presence of a FLR between each pair of stations. Pairs of stations at lower latitudes give higher resonant frequencies (respectively 3, 3.4, 4.4, 6 mHz) as one would expect for shorter field lines and higher field strengths (this effect dominates on the dayside (Archer et al., 2015; Archer & Plaschke, 2015)), with those closest to the GOES foot-points showing a resonance near the frequency of the compressional wave observed in space. When applying this method to an earlier interval, 17:30 to 17:50, we do not find clear evidence indicating the presence of FLRs. Plots for this time interval can be found in the SI document (Figures S2a and S2b in Supporting Information S1).

4.4. Magnetopause Motion

Between 17:57 and 18:08, shortly after the arrival of the ST, we observe field reversals in the *Z* components of the magnetic field observed by THEMIS A, D, and E, indicating that the spacecraft crossed the magnetopause (see Figure 1d). With the magnetometer data, we identify a singular crossing for THA and three crossings each for THD and THE, which were both located further out; the crossing times are included in Table 2. In the cases where multiple B_z fluctuations between positive and negative values were observed within a few seconds, we consider only the last crossing. We then apply MVA on each crossing to determine the magnetopause normal vector at that time and location, using a two-minutes interval centered around each crossing. The derived magnetopause normals and corresponding eigenvalue ratios are also included in Table 2.

Table 2
Magnetopause Crossings Information for THEMIS A, D, and E

Time	Spacecraft	Crossing direction	Magnetopause normal	λ_M/λ_N
17:57:18	THD	outbound	[0.84, 0.47, 0.26]	9.9
18:02:15	THE	outbound	[0.97, 0.19, 0.15]	2.0
18:03:40	THE	inbound	[0.78, 0.54, 0.31]	2.4
18:03:49	THD	inbound	[0.79, 0.54, 0.29]	3.4
18:06:36	THD	outbound	[0.87, 0.44, 0.21]	10.2
18:07:15	THE	outbound	[0.95, 0.28, 0.11]	3.8
18:07:50	THA	outbound	[0.84, 0.43, 0.32]	4.0

Note. The magnetopause normal, derived from MVA, is given in GSM coordinates. λ_M/λ_N is the ratio between the middle and minimum eigenvalues.

The multiple crossings for THD and THE suggest that the magnetopause was oscillating. The consecutive THE outbound crossings, more regular than the THD ones, indicate an oscillation frequency of 3.3 mHz, similar to the frequency observed at geosynchronous orbit. Considering consecutive THD outbound crossings would instead yield a frequency of 1.8 mHz. However, we do not observe clear Pc5 oscillations in the magnetic field data; despite this, the FFTs of the data from 17:20 to 17:55, band-pass filtered between 2 and 6 mHz, show consistent peaks at 2.41 mHz in all spacecraft, which doesn't however match the 3.03 mHz frequency observed at GOES 13 and 15. The

21699402, 2026, 8, Downloaded from https://agupubs.onlinelibrary.wiley.com/doi/10.1029/2025JA035007 by Imperial College London, Wiley Online Library on [03/08/2026]. See the Terms and Conditions (https://onlinelibrary.wiley.com/terms-and-conditions) on Wiley Online Library for rules of use; OA articles are governed by the applicable Creative Commons License

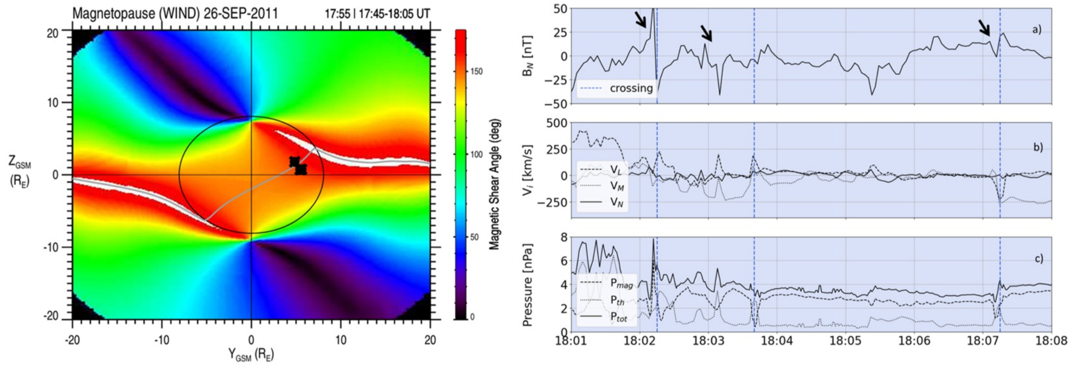

Figure 9. On the left, Maximum Magnetic Shear Model showing the location of the reconnection X line (gray) and that of THA, THD, and THE (black symbols). On the right, THEMIS E (a) N component of the magnetic field, (b) ion velocities in LMN components, and (c) magnetic, plasma and total pressure. Magnetopause crossings are indicated by the vertical dashed lines, while flux transfer events signatures are highlighted by black arrows.

THEMIS magnetic field data and its corresponding FFTs are shown in the SI document (Figures S3a–S3d in Supporting Information S1).

It is clear that the normal vectors obtained from all three THEMIS crossings are closely aligned, with the exception of the first and last crossings for THE (at 18:02:15 and 18:07:15 respectively). While the angles between the normals from these THE crossings and the others range approximately between 12 and 25°. The angles between the remaining normals range between 2 and 10°. Visual inspection of the magnetic field data shows that, near the first and last THE crossings, the GSM B_x component presented bipolar signatures, a potential indicator of Flux Transfer Event (FTE) observations. Transforming the data into LMN coordinates, where N is the average normal vector obtained from MVA, M is perpendicular to N and GSM Z (i.e., points dawnward), and L is perpendicular to both N and M (and points approximately northward) (Russell & Elphic, 1978), we confirm the presence of FTE-like signatures - bipolar signature in B_N, maxima in $P_{mag} + P_{th}$ (Paschmann et al., 1982) - and ion jets in the L direction. These signatures are observed both in THE (see Figure 9b) and THD (not shown). In addition to this, we run the Maximum Magnetic Shear model (Trattner et al., 2007) to determine the expected location of the reconnection X line on the magnetopause. The output of the model is shown in Figure 9a. At 17:55 the THEMIS satellites are located at the predicted location of the dayside magnetopause X-line which is in agreement with the observed reconnection signatures discussed above. The vicinity and relative position of the THEMIS spacecraft to the reconnection X-line can explain the presence of oppositely directed jets in the north-south (L) direction displayed in Figure 9 (right).

To examine the large-scale variation in the magnetopause during this event, we simulated it with the Space Weather Modelling Framework (SWMF) (Tóth et al., 2005) provided by NASA's Community Coordinated Modelling Center (CCMC). MHD simulations provide us with information about the global behavior of the magnetopause and with the ability to determine how different solar wind parameters affect this boundary. We performed two simulation runs: one with the ST (run1) and one without it (run2). The simulation results are shown in Figure S4 in Supporting Information S1. The run1 output gives good agreements between the simulated and observed THEMIS magnetic field data, although it does not capture the multiple magnetopause crossings of THD and THE. In *run1* the simulated magnetopause nose is located at approximately 9.8 R_E at 17:44, and it moves down to 7.9 R_E by 18:00. The FFT on the magnetopause nose location between 17:40 and 18:40, first band-pass filtered between 1 and 8 mHz, yields a large peak at 1.37 mHz (likely from the pressure variations observed by ARTEMIS), and only small peaks at 2.19 and 3.28 mHz. Conversely, in run2, in which we keep the IMF northward throughout the event, we do not observe any simulated magnetopause crossings by THEMIS. This implies that the global inward motion of the magnetopause was caused not by an increase in dynamic pressure or by the outbound motion of the spacecraft, but by magnetopause erosion under southward IMF. At the same time, the lack of multiple crossings in THD and THE simulated data suggests that the MHD models do not provide a complete picture, due to other processes not being captured or because of the model's limited spatial resolution. This extends to the ULF waves, which are also not observed in the simulated magnetic fields along the G13 and G15 orbits.

21699402, 2026, 8, Downloaded from https://agupubs.onlinelibrary.wiley.com/doi/10.1029/2025JA035007 by Imperial College London, Wiley Online Library on [03/08/2026]. See the Terms and Conditions (https://onlinelibrary.wiley.com/terms-and-conditions) on Wiley Online Library for rules of use; OA articles are governed by the applicable Creative Commons License

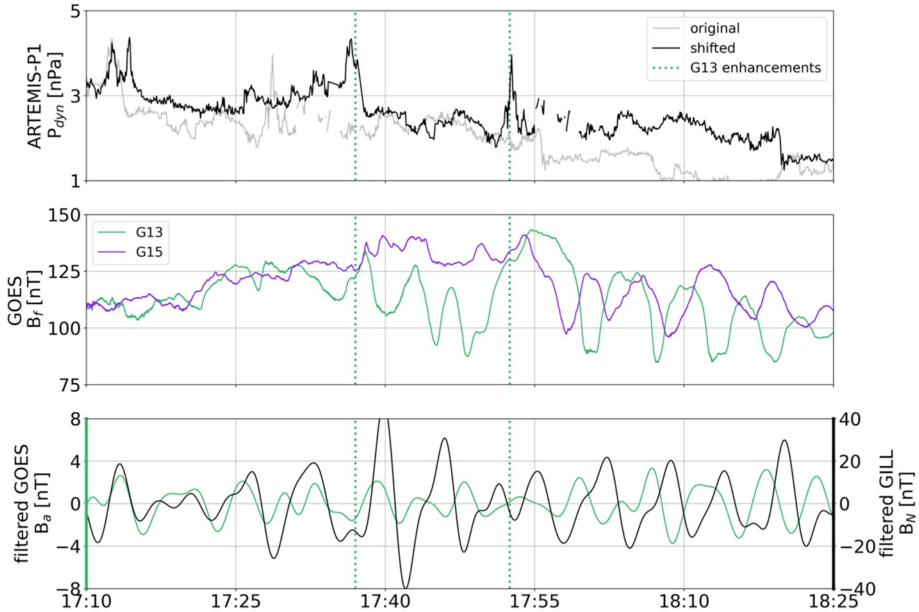

Figure 10. At the top, the solar wind P_{dyn} (original and time-shifted by 25 min), in the middle GOES 13 and 15 B_f components, and, at the bottom, the GOES 13 B_a and Gillam B_N components, both filtered in the 2–6 mHz range. The G13 wave power enhancements at 17:37 and 17:53 are indicated by the vertical dotted lines.

5. Discussion

In the previous section, we examined the solar wind and IMF conditions observed by ARTEMIS, as well as the magnetospheric observations obtained from the GOES and THEMIS spacecrafts and ground magnetometer stations. We found the ULF waves observed by GOES to be mostly compressional, with small radial and azimuthal oscillations. Spectral analysis yielded a peak frequency of 3.03 mHz, allowing us to classify the waves as Pc5. We found no evidence of this frequency within the ARTEMIS P1 dynamic pressure and IMF B_z data we analysed. Ground magnetometer data near the GOES foot-points revealed Pc5 oscillations at similar frequencies and evidence of FLRs following the spike's arrival. We found no evidence of magnetic field variations at the 3.03 mHz frequency near the magnetopause, in THEMIS data. However, when examining the THEMIS magnetopause crossings, we determined the presence of magnetopause oscillations at 3.3 mHz and of potential flux transfer events (FTEs) signatures. In this section, we will discuss physical mechanisms which can explain both the ULF waves observed at geosynchronous orbit and the ground.

5.1. Effects of Solar Wind Dynamic Pressure Spikes

Transient dynamic pressure pulses are often associated with ULF wave driving (e.g., Eriksson et al., 2006; Xie et al., 2023; Zhang et al., 2010) and, as shown in Figure 1, ARTEMIS-P1 detected a clear dynamic pressure spike at 17:28, as the IMF switched from northward to southward. The dynamic pressure increased from ∼2 nPa to ∼4 nPa, a twofold increase. Shortly before this spike, at 17:12, ARTEMIS-P1 observed another spike where the dynamic pressure initially increased by ∼1 nPa and then dropped by ∼2 nPa. The 25 min solar wind propagation described in Section 3 yields arrival times at the magnetopause of 17:37 for the first spike and 17:53 for the second spike. At 17:37 the SYM-H index increases sharply by ∼10 nT, and THEMIS A, D, and E all appear to be pushed from the inner magnetosphere into the LLBL, suggesting that a pressure spike might have compressed the magnetopause. Additional plots of THEMIS data, including ion energy spectrograms showing the inner magnetosphere-LLBL transitions, are available in the SI document (Figures S3a–S3c in Supporting Information S1). Shortly after, at 17:39 we also see an enhancement of Pc5 oscillations at the Churchill line magnetometers stations. The estimated arrival times for the two spikes show very good agreement with the enhancements in wave power of GOES 13 and 15, as shown in Figure 10. Notably, the two pressure spikes were not apparent in the 1 min OMNI data, highlighting the importance of high-resolution solar wind data near Earth in examining the source of activity within the magnetosphere.

21699402, 2026, 8, Downloaded from https://agupubs.onlinelibrary.wiley.com/doi/10.1029/2025JA035007 by Imperial College London, Wiley Online Library on [03/08/2026]. See the Terms and Conditions (https://onlinelibrary.wiley.com/terms-and-conditions) on Wiley Online Library for rules of use; OA articles are governed by the applicable Creative Commons License

The correlation in timing between the pressure spikes and the wave activity at GOES indicates that these spikes were likely the drivers. Notably, the spike associated with the ST appears to drive a more global wave and causes a distinct change to the FLR signature. It is also this combination of spike and ST that leads to the erosion of the magnetopause, as demonstrated by our simulations, including a null experiment.

5.1.1. Magnetospheric Compression Giving Rise to Drift-Mirror Instability

The drift-mirror instability drives Pc5 ULF waves in plasmas with pressure anisotropy and high (>1) plasma $\beta_\perp$ (Hasegawa, 1969), and has been observed at the bowshock and the magnetosheath (Gary et al., 1993; Lacombe & Belmont, 1995), and also in the Earth's magnetosphere (e.g., Constantinescu et al., 2009; Korotova et al., 2020; Rae, Mann, et al., 2007; Soto-Chavez et al., 2019).

To determine whether the conditions for the instability are met, Hasegawa, 1969 identified a threshold, Γ_{DM}:

$$\Gamma_{DM} = 1 + \beta_\perp\left(1 - \frac{T_\perp}{T_\parallel}\right) < 0 \quad (1)$$

where $T_\perp, T_\parallel$ are the perpendicular and parallel temperatures and $\beta_\perp = (n_e k_B T_{e\perp} + n_i k_B T_{i\perp})/(B^2/2\mu_0)$. GOES 13 and 15 do not measure the thermal plasma density and temperature so we are not able to measure particle temperatures and densities and apply this test. Although Cooper et al., 2021 found that the plasma β conditions for the instability (β >1) were only present in the dusk-midnight sector for $L < 6$, just inside geosynchronous orbit, other studies (e.g., Korotova et al., 2020; Takahashi et al., 1985) have presented a detection of drift-mirror waves at geosynchronous orbit near noon. In Korotova et al., 2020, the compressional wave amplitudes reached 16 nT under strong magnetospheric compression, slightly smaller than the amplitudes observed in this case study.

Drift-mirror waves are characterized by magnetic field and thermal pressure oscillations in anti-phase, so that the total pressure remains approximately constant (e.g., Rae, Mann, et al., 2007; Soto-Chavez et al., 2019). Although ion and electron density data are not available, we use 1-min electron fluxes for 40 and 75 keV electrons provided by EPS-MAGED as an approximation of electron densities. We note that these fluxes are for energetic electrons that do not necessarily represent the lower-energy population which dominates the plasma pressure. As shown in Figure 11, for both GOES 13 and 15 we observe intervals during which the magnetic field magnitude and the integral fluxes are in anti-phase. The 180° phase difference is clearest between 18:00 and 18:35 for both GOES spacecraft. It is worth noting that, for GOES 13, at each energy, different telescopes presented different phase differences with no apparent connection to their look-direction. While both electron and ion populations can contribute to the instability, we have no available ion data to examine.

The propagation direction of drift-mirror waves is expected to depend on the pressure gradient, being westward for an inward-pointing gradient (Takahashi et al., 1985). The propagation is also expected to be at the ion curvature gradient drift velocity and, hence, the delay in magnetic field observations between GOES 13 and GOES 15 may be attributed to the wave's westward motion at low speed. However, the good agreement between the timings of the enhancement of oscillations at GOES 13, the start of oscillations at GOES 15, and the arrival of the second pressure spike, suggests that the latter may have contributed to the spreading of pressure anisotropy. The more localised nature of this driver would explain the absence of waves at the THEMIS spacecraft, located further out in the post-noon region.

We believe the drift-mirror instability to be the most likely candidate to drive the observed compressional waves. However, we lack the necessary instruments to determine whether the conditions necessary for the instability to arise were present. The excitation of temperature anisotropies that give rise to ULF waves is not a new suggestion. Anderson et al., 1990 used AMPTE-CCE observations to show that Electromagnetic Ion Cyclotron (EMIC) waves are most commonly observed at, or close to, the dayside magnetopause, as well as in the inner magnetosphere. Many studies have discussed that there may be two discrete ways to generate the requisite temperature anisotropy to drive such waves; substorm injection in the inner magnetosphere giving rise to enhanced T_{perp} (Cooper et al., 2021; Ge et al., 2011; Korotova & Sibeck, 2024), and the compression of the dayside magnetopause at higher L-shells increasing the local T_{perp} (Anderson & Hamilton, 1993; Usanova et al., 2008, 2012). Given that mirror modes grow off of the same temperature anisotropy as EMIC waves ($T_{perp}/T_{parallel} > 1$) then it is logical that the same would be true for drift-mirror waves. Here, we show both a temporal link from the first

21699402, 2026, 8, Downloaded from https://agupubs.onlinelibrary.wiley.com/doi/10.1029/2025JA035007 by Imperial College London, Wiley Online Library on [03/08/2026]. See the Terms and Conditions (https://onlinelibrary.wiley.com/terms-and-conditions) on Wiley Online Library for rules of use; OA articles are governed by the applicable Creative Commons License

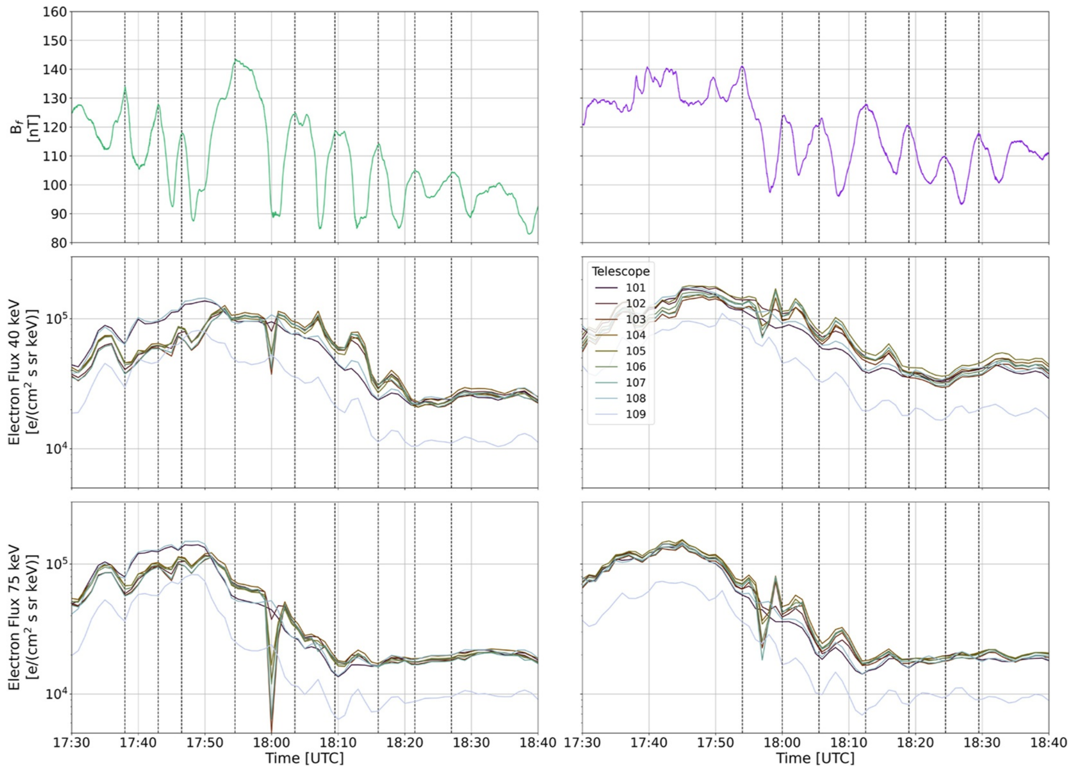

Figure 11. Field-aligned magnetic field data and electron fluxes for 40 and 75 keV electrons for GOES 13 (left column) and GOES 15 (right column). The different colored lines represent fluxes measured by different telescopes.

pressure spike for the generation of drift-mirror waves, and an enhancement of the spatial extent of the anisotropy region from the second pressure spike. Previous studies have concentrated primarily on the outer magnetosphere (e.g., Baumjohann et al., 1987; Constantinescu et al., 2009; Rae, Mann, et al., 2007). Our study shows that drift-mirror instabilities can occur via pressure spike in the geosynchronous region, providing a link between the solar wind, outer magnetosphere and inner magnetosphere that could be significant for ring current and radiation belt physics.

5.1.2. Excitation of Field Line Resonances

Field Line Resonances are standing waves generated by the reflection of shear Alfvén waves at the ionospheres (Chen & Hasegawa, 1974b; Southwood, 1974). FLRs can be excited by coupling with compressional waves oscillating at the field line's natural frequency (e.g., Chen & Hasegawa, 1974b; Kivelson & Southwood, 1986), which depends on the field line's length, plasma density and magnetic field conditions (e.g., Singer et al., 1981). Previous studies have investigated the coupling between the drift-mirror mode and standing Alfvén waves, suggesting its observation (e.g., Pokhotelov et al., 1985; Rae, Mann, et al., 2007; Woch et al., 1988).

The analysis of Churchill line magnetometers conducted in Section 4.3 revealed wave power enhancements which are well-aligned with the expected arrival of the pressure spikes at the magnetosphere, as shown in Figure 6. The responses to the two spikes were however different; the first spike led to a wave power enhancement in both the B_N and B_E components, while the ST-associated spike resulted in a significant power enhancement only in the B_N component. Additionally, it was only after the second spike that clear FLR signatures were observed, and that clearer oscillations in the radial and azimuthal magnetic field components were observed at the GOES spacecraft.

When observed from the ground, FLR characteristics are modified by the interaction with the ionosphere, which leads to a 90° left-handed rotation in polarisation (Hughes & Southwood, 1976). Taking this into account, the predominance of oscillations in the N component at the ground should approximately translate to an azimuthal oscillation in space. The azimuthal oscillations at GOES are however rather weak, which may suggest that the

21699402, 2026, 8, Downloaded from https://agupubs.onlinelibrary.wiley.com/doi/10.1029/2025JA035007 by Imperial College London, Wiley Online Library on [03/08/2026]. See the Terms and Conditions (https://onlinelibrary.wiley.com/terms-and-conditions) on Wiley Online Library for rules of use; OA articles are governed by the applicable Creative Commons License

fundamental mode, characterized by a node in the transverse components at the equator (Hughes, 1994), is being observed. We find particularly good correlation ($r = 0.74$) between G13 B_A and Gillam B_N in the interval between 17:53 and 18:25 and for a lag of 2 min (see Figure 10, bottom panel), suggesting a potential coupling between standing Alfvén waves and drift-mirror modes after the arrival of the ST.

5.2. Discussion of Other Potential Driving Mechanisms

While the observations as presented are suggestive of a drift-mirror mode wave coupling to an FLR following solar wind pressure spikes and a ST of the IMF, the evidence is not conclusive. In this Section, we present other common ULF drivers and discuss their feasibility as driving mechanisms for the observed waves.

5.2.1. Global Magnetospheric Modes

The pressure spikes observed by ARTEMIS-P1 are broadband impulses. Wright & Rickard, 1995 determined that broadband fluctuations in the solar wind may be filtered by the magnetospheric cavity when its eigenfrequencies are within the driving spectrum. This implies that pressure spikes can excite monochromatic fast magnetosonic waves which become trapped between the sharp density gradients represented by magnetospheric boundaries such as the magnetopause or the plasmapause, giving rise to the standing compressional waves commonly referred to as "global modes" (Kivelson & Southwood, 1985). These modes are commonly classified into two categories, cavity modes and waveguide modes (Samson et al., 1992), based on whether the magnetosphere is assumed to be closed or open, respectively. They are usually associated with frequencies above 5 mHz, a threshold higher than our 3.03 mHz observed frequency, however lower frequencies are supported by models allowing quarter-wavelength modes (Mann et al., 1999; Sibeck, 2004).

The first solar wind pressure spike could have contributed to the excitation of a cavity/waveguide mode, observed as compressional oscillations in G13 magnetic field data. MVA suggested that the ST-associated spike first hit the magnetopause in the post-noon region, but we have no such information regarding the first pressure spike. The initial detection of waves only at G13 might suggest that the spike hit the magnetopause at an MLT similar to that of the spacecraft, that is, in the post-noon region. The second pressure spike, associated with the southward IMF turning, could have caused not only a large wave power enhancement in G13 compressional oscillations, but also an increase in the spatial extent of the standing waves, as suggested by the detection of waves at G15 shortly after the spike's arrival. However, the difference in observations between the GOES spacecraft makes the global mode hypothesis unlikely, since a global mode should have large-scale structure and high propagation speeds (~500 km s^{-1}). In addition to this, we did not observe clear evidence of waves at the THEMIS location. Elsden & Wright, 2019 showed that an external driver impinging asymmetrically on the magnetopause may result in the excitation of partially standing (near noon) and partially propagating (near the flanks) waves, depending on the local time. However, we believe that an explanation involving a more localised phenomenon, such as the drift-mirror instability, seems more likely when considering other cavity/waveguide mode properties. Observations of global modes (e.g., Eriksson et al., 2006; Hartinger et al., 2012, 2023; Kivelson et al., 1997) are rather rare because of some of the waves' characteristics which make their detection difficult. Among the factors making cavity modes challenging to observe, Kivelson et al., 1997 identified their quick damping and small amplitudes, often less than 1 nT (Hartinger, Turner, et al., 2013). While recent studies such as Takahashi et al., 2018; Takahashi et al., 2023 have found evidence of shock-driven standing fast mode waves with larger amplitudes, the events reported in these papers involve interplanetary shocks with larger increases in dynamic pressure. This further suggests the waves observed in this event are not global modes.

5.2.2. Quasi-Periodic Solar Wind Fluctuations

Monochromatic quasi-periodic fluctuations in the solar wind dynamic pressure have been found to drive compressional ULF waves at the same frequency within the magnetosphere (e.g.., Kepko et al., 2002; Kepko & Spence, 2003; Stephenson & Walker, 2002; Viall et al., 2009). The FFT of solar wind dynamic pressure observed by ARTEMIS-P1 does not reveal monochromatic oscillations at the same frequency observed at G13 and G15, nor does it show significant power in the 2–6 mHz range. Hence, it seems very unlikely that the ULF waves observed at geosynchronous orbit were driven by solar wind dynamic pressure periodic fluctuations.

As a final consideration regarding driving by solar wind pressure, we must take into account that pressure fluctuations, whether periodic or transient, can be generated in the magnetosheath due to the interaction of the

21699402, 2026, 8, Downloaded from https://agupubs.onlinelibrary.wiley.com/doi/10.1029/2025JA035007 by Imperial College London, Wiley Online Library on [03/08/2026]. See the Terms and Conditions (https://onlinelibrary.wiley.com/terms-and-conditions) on Wiley Online Library for rules of use; OA articles are governed by the applicable Creative Commons License

solar wind with the bow shock or foreshock, and that these can in turn generate magnetospheric Pc5 waves (e.g., Fairfield et al., 1990; Hartinger, Turner, et al., 2013; B. Wang et al., 2020). For this event, we have no magnetosheath observations to corroborate this, so we cannot rule it out. However, the lack of evidence of waves just inside the magnetopause by THEMIS prior to their magnetopause crossing mean that the transmission of any magnetosheath waves is unlikely.

5.2.3. Magnetopause Surface Eigenmodes

Magnetopause Surface Eigenmodes (MSEs) or Kruskal-Schwarzschild (KS) modes are standing waves on the magnetopause surface, formed by fast surface waves traveling in opposite directions along the field lines and reflecting at the north and south ionospheres (Plaschke & Glassmeier, 2011). They can be excited by localised pressure pulses, magnetosheath jets, or interplanetary shocks. MSEs have only been directly observed recently through multi-point measurements (Archer et al., 2019). However, a link between them and compressional magnetospheric ULF waves had previously been established (e.g., Plaschke et al., 2013). Given the scarcity of direct MSEs observations, theoretical calculations and modeling have been used to understand their properties (e.g., Archer et al., 2023; Hartinger et al., 2015; Plaschke & Glassmeier, 2011). Through MHD modeling with the SWMF, Hartinger et al., 2015 found that the fundamental mode, which the agreement between the magnetopause normals obtained by the THEMIS would suggest (see Section 4.4), is expected to generate ULF waves which are predominantly compressional at the equator and transverse near the ionospheres, with amplitudes decaying with distance from the magnetopause. Numerical modeling from Archer & Plaschke, 2015 suggests that for the magnetospheric densities observed by THEMIS, the MSE frequency for our event would be in the 2.6–3.4 mHz range, which matches well the 3.03 mHz frequency observed at GOES. However, the large observed wave amplitudes (20 nT) may be incompatible with those of ULF waves excited by MSEs. Furthermore, although the ground signatures of MSEs are not fully understood, MHD simulations have suggested that, near noon, they would be polarised in the East-West direction of the magnetic field and constant frequency across L-shells (Archer et al., 2021, 2023), which is not in agreement with our observations.

5.2.4. Magnetic Reconnection

The arrival of the ST at the magnetosphere marks the beginning of an extended period (~1 hr 30 min) of southward IMF, which is expected to drive magnetic reconnection at the dayside magnetopause. Under southward IMF, the magnetopause has been found to be more oscillatory than under northward IMF, suggesting that reconnection contributes to magnetopause surface waves (Song et al., 1988). Additionally, despite some early controversy (see Gillis et al., 1987; Lanzerotti, 1988), *transient* reconnection, in the form of FTEs (Paschmann et al., 1982; Russell & Elphic, 1978), has been identified as a driver of Pc5 activity. It has been suggested that, as these structures move tailward along the magnetopause flanks, their motion leads to magnetopause oscillations which in turn cause compressional fast mode waves to enter the magnetosphere and excite ULF pulsations (e.g., Bentley et al., 2018; Hwang & Sibeck, 2016; Liu et al., 2008; Russell & Elphic, 1978). Moreover, the mean occurrence rate of FTEs has been found to be approximately 8 min, i.e., in the Pc5 range (e.g., Kuo et al., 1995; Rijnbeek et al., 1984).

Observations of reconnection-related Pc5 pulsations are relatively scarce, and have been reported in Glasmeier et al., 1984, Prikryl et al., 1998; Le et al., 2004; Glasmeier et al., 1984 describes the observation of large amplitude Pc5 waves at geosynchronous orbit and at the ground. However, what they attribute to FTEs is only an isolated Pc5 wave packet, and not a long-lasting pulsation, as in our event. Le et al., 2004, which also described observations of localised Pc5 waves at geosynchronous orbit and at the ground, also attributed transient pulsations to FTEs, and the more long-lasting oscillations to magnetopause oscillations due to pulsed reconnection.

As discussed in Section 4.4, the Maximum Magnetic Shear Model suggested that, at the time of our event, the THEMIS spacecraft were located near the reconnection *X* line, and that both THD and THE observed bipolar signatures in B_N and peaks in total pressure, which are typical features of FTE observations (Paschmann et al., 1982). However, while THEMIS did observe FTE-like signatures, the period of southward IMF and the manifestation of these features only began ~20 min after the beginning of the ULF pulsations. In addition to that, the periodicity of FTEs observations from THEMIS D (<5 min for THD), does not match that of the ULF waves observed at GOES 13 and 15, and hence we cannot provide a definitive link between the two. Finally, we do not

21699402, 2026, 8, Downloaded from https://agupubs.onlinelibrary.wiley.com/doi/10.1029/2025JA035007 by Imperial College London, Wiley Online Library on [03/08/2026]. See the Terms and Conditions (https://onlinelibrary.wiley.com/terms-and-conditions) on Wiley Online Library for rules of use; OA articles are governed by the applicable Creative Commons License

21699402, 2026, 8, Downloaded from https://agupubs.onlinelibrary.wiley.com/doi/10.1029/2025JA035007 by Imperial College London, Wiley Online Library on [03/08/2026]. See the Terms and Conditions (https://onlinelibrary.wiley.com/terms-and-conditions) on Wiley Online Library for rules of use; OA articles are governed by the applicable Creative Commons License

observe significant IMF B_z fluctuations in ARTEMIS P1 data, which would be needed to indicate that a pulsed reconnection rate might be driving the ULF waves.

5.2.5. Kelvin Helmholtz Instability

The KH instability, which is known to generate anti-sunward waves on the magnetopause flanks, has been found to excite monochromatic compressional waves/global modes and FLRs in the Pc4/5 frequency range (e.g., Bentley et al., 2018; Chen & Hasegawa, 1974b; Claudepierre et al., 2008; Mann et al., 2002; Rae et al., 2005; Rae, Watt, et al., 2007).

While KH waves can be generated under southward IMF, a statistical study by Kavosi & Raeder, 2015 found that they have a very low occurrence rate for the clock angle observed during this event (∼140°). The magnetopause is also expected to be stable against the KH instability near the subsolar point, where the velocity shear is lower (Farrugia et al., 1998; Sen, 1965), and the consistent quasi-radial magnetopause normals obtained from MVA (see Table 2) are not compatible with KH waves. Finally, a characteristic of ULF waves driven by the KH instability is that both their polarisation and propagation direction reverse at noon, with the waves propagating westward in the morning sector and eastward in the afternoon sector (e.g., Olson & Rostoker, 1978). This does not match our observations of a westward propagating wave in the post-noon sector. Hence, we do not expect the observed compressional waves or the magnetopause oscillations to be generated by this mechanism.

5.2.6. Drift-Bounce Resonance

Drift-bounce resonance is a wave-particle interaction commonly associated with the excitation of ULF waves. In this process, energetic particles (e.g., ring current ions) with an unstable distribution contribute to the growth of high-m poloidal waves (Southwood et al., 1969; Southwood & Kivelson, 1982). Drift-bounce resonance is an internal mechanism usually associated with periods of geomagnetic activity such as the recovery phase of storms (e.g., Nagano & Araki, 1983; Ozeke & Mann, 2008); we note that the pulsations in our event began while the Dst index was low but increasing before the arrival of the ST.

Characteristic signatures of this process would be a ULF wave with a strong radial component and a 180° phase difference between ion fluxes above and below the resonant energy (Southwood & Kivelson, 1981). Due to the lack of ion data from GOES, we could not determine the presence of such a phase difference between ion fluxes. While the waves observed by GOES 13 and 15 do have a significant radial component, the amplitude of the poloidal oscillations (∼10–15 nT) is small compared to that of the field-aligned oscillations (varying between ∼20–30 nT). Hartinger et al., 2012, examining similar circumstances, found this to be inconsistent with drift-bounce resonance theory. We also note that the magnetic field amplitudes of Pc5 waves attributed to drift-bounce resonance in previous studies (e.g., Claudepierre et al., 2013; Dai et al., 2013; Hao et al., 2014) appear to have significantly smaller amplitudes than in our event. Despite this, the lack of ion data prevents us from fully ruling out drift-bounce resonance as an excitation mechanism of the ULF waves.

6. Conclusions

In this paper, we presented the analysis of large amplitude, narrowband oscillations observed near noon at geosynchronous orbit by the GOES 13 and 15 spacecraft. We classified the oscillations as Pc5 ULF waves with frequency 3.03 mHz, and found them to be mostly compressional, although also accompanied by smaller radial and azimuthal oscillations at the same frequency.

We suggested a link between the driving mechanism and the arrival of two consecutive solar wind dynamic pressure spikes at the dayside magnetopause. The first spike's arrival at the boundary appeared to be followed by particularly large amplitude (∼20 nT) compressional waves at GOES 13, while the arrival of the second pressure spike, associated with a large ST, coincided with a wave power enhancement at GOES 13 and the observed start of wave activity at GOES 15. Following the second spike, we also observed periodic magnetopause crossings at a similar frequency (3.3 mHz) in THEMIS D and E data, located in the post-noon magnetosphere; however, no significant oscillations in magnetic field were observed at these spacecraft. Finally, we analysed ground data collected by Churchill line magnetometer stations, which were located near the GOES foot-points. We found wave power enhancements in the eastward and northward components of the magnetic field following the spikes, and a slight change in polarisation following the ST-associated spike. Furthermore, after this spike we found

21699402, 2026, 8, Downloaded from https://agupubs.onlinelibrary.wiley.com/doi/10.1029/2025JA035007 by Imperial College London, Wiley Online Library on [03/08/2026]. See the Terms and Conditions (https://onlinelibrary.wiley.com/terms-and-conditions) on Wiley Online Library for rules of use; OA articles are governed by the applicable Creative Commons License

evidence of FLR in the northward component, which are well correlated ($r = 0.72$) with the azimuthal oscillations observed by GOES 13, suggesting coupling between the compressional wave and the standing Alfvén mode. One important factor in examining the source of these waves was the high time resolution solar wind observations from ARTEMIS since the pressure spikes were not apparent in the OMNI data set.

We considered different potential driving mechanisms, both internal and external, and found the most likely driver to be the drift-mirror instability, excited by the compression of the magnetopause by the solar wind pressure spikes. While the wave properties and the manner of their occurrence suggest the drift-mirror instability, we were not able to fully confirm the link between the observed waves and this driving mechanism due to the lack of relevant instruments onboard the GOES spacecraft.

Conflict of Interest

The authors declare no conflicts of interest relevant to this study.

Availability Statement

GOES and THEMIS data are available through NASA's CDAWeb (https://cdaweb.gsfc.nasa.gov/). Ground magnetometer data are available through the SuperMAG collaboration (https://supermag.jhuapl.edu/). Outputs of the SWMF model runs (*Chiara_Lazzeri_042825_1*, *Chiara_Lazzeri_042825_2*) are available at https://ccmc.gsfc.nasa.gov.

Acknowledgments

CL acknowledges STFC's support through the PhD degree (ST/X508858/1). CF acknowledges NERC's support (NE/V002724/1). AS is supported by the UK Space Agency under Grant ST/T002964/1 and partly supported by the International Space Science Institute (ISSI). AF acknowledges STFC's support (ST/W001004/1). MA was supported by UKRI Future Leaders Fellowship (MR/X034704/1). The research at LASP was supported by the MMS prime Grant (NNG04EB99C). JR is supported by STFC (Grant ST/X001008/1) and NERC NE/W003198/1. AD is supported by NSFC Grant 42350710200 and Shandong Provincial Govt ("Double Hundred Talent Plan"): WSR2023038″ We acknowledge NASA contract NAS5-02099 and V. Angelopoulos for use of data from the THEMIS Mission. Specifically: K. H. Glassmeier, U. Auster and W. Baumjohann for the use of FGM data provided under the lead of the Technical University of Braunschweig and with financial support through the German Ministry for Economy and Technology and the German Center for Aviation and Space (DLR) under contract 50 OC 0302, C. W. Carlson and J. P. McFadden for use of ESA data. This work was carried out using the SWMF and BATS-R-US tools developed at the University of Michigan's Center for Space Environment Modeling. The modeling tools described in this publication are available online through the University of Michigan for download and are available for use at the CCMC (https://ccmc.gsfc.nasa.gov).

References

Alken, P., Thébault, E., Beggan, C. D., Amit, H., Aubert, J., Baerenzung, J., et al. (2021). International Geomagnetic Reference Field: The thirteenth generation. *Earth Planets and Space*, *73*(1), 49. https://doi.org/10.1186/s40623-020-01288-x

Anderson, B. J., & Hamilton, D. C. (1993). Electromagnetic ion cyclotron waves stimulated by modest magnetospheric compressions. *Journal of Geophysical Research*, *98*(A7), 11369–11382. https://doi.org/10.1029/93JA00605

Anderson, B. J., Takahashi, K., Erlandson, R. E., & Zanetti, L. J. (1990). Pc1 pulsations observed by AMPTE/CCE in the Earth's outer magnetosphere. *Geophysical Research Letters*, *17*(11), 1853–1856. https://doi.org/10.1029/GL017i011p01853

Angelopoulos, V. (2011). The ARTEMIS Mission. *Space Science Reviews*, *165*(1), 3–25. https://doi.org/10.1007/s11214-010-9687-2

Archer, M. O., Hartinger, M. D., Plaschke, F., Southwood, D. J., & Rastaetter, L. (2021). Magnetopause ripples going against the flow form azimuthally stationary surface waves. *Nature Communications*, *12*(1), 5697. https://doi.org/10.1038/s41467-021-25923-7

Archer, M. O., Hartinger, M. D., Rastätter, L., Southwood, D. J., Heyns, M., Eggington, J. W. B., et al. (2023). Auroral, ionospheric and ground magnetic signatures of Magnetopause surface modes. *Journal of Geophysical Research: Space Physics*, *128*(3), e2022JA031081. https://doi.org/10.1029/2022JA031081

Archer, M. O., Hartinger, M. D., Walsh, B. M., Plaschke, F., & Angelopoulos, V. (2015). Frequency variability of standing Alfvén waves excited by fast mode resonances in the outer magnetosphere. *Geophysical Research Letters*, *42*(23), 10150–10159. https://doi.org/10.1002/2015GL066683

Archer, M. O., Hietala, H., Hartinger, M. D., Plaschke, F., & Angelopoulos, V. (2019). Direct observations of a surface eigenmode of the dayside magnetopause. *Nature Communications*, *10*(1), 615. https://doi.org/10.1038/s41467-018-08134-5

Archer, M. O., & Plaschke, F. (2015). What frequencies of standing surface waves can the subsolar magnetopause support? *Journal of Geophysical Research: Space Physics*, *120*(5), 3632–3646. https://doi.org/10.1002/2014JA020545

Auster, H. U., Glassmeier, K. H., Magnes, W., Aydogar, O., Baumjohann, W., Constantinescu, D., et al. (2008). The THEMIS fluxgate magnetometer. *Space Science Reviews*, *141*(1), 235–264. https://doi.org/10.1007/s11214-008-9365-9

Baumjohann, W., Sckopke, N., LaBelle, J., Klecker, B., Lühr, H., & Glassmeier, K. H. (1987). Plasma and field observations of a compressional Pc 5 wave event. *Journal of Geophysical Research*, *92*(A11), 12203–12212. https://doi.org/10.1029/JA092iA11p12203

Bentley, S. N., Watt, C. E. J., Owens, M. J., & Rae, I. J. (2018). ULF wave activity in the magnetosphere: Resolving solar wind interdependencies to identify driving mechanisms. *Journal of Geophysical Research: Space Physics*, *123*(4), 2745–2771. https://doi.org/10.1002/2017JA024740

Chen, L., & Hasegawa, A. (1974a). A theory of long-period magnetic pulsations: 2. Impulse excitation of surface eigenmode. *Journal of Geophysical Research (1896-1977)*, *79*(7), 1033–1037. https://doi.org/10.1029/JA079i007p01033

Chen, L., & Hasegawa, A. (1974b). A theory of long-period magnetic pulsations: 1. Steady state excitation of field line resonance. *Journal of Geophysical Research (1896-1977)*, *79*(7), 1024–1032. https://doi.org/10.1029/JA079i007p01024

Claudepierre, S. G., Elkington, S. R., & Wiltberger, M. (2008). Solar wind driving of magnetospheric ULF waves: Pulsations driven by velocity shear at the magnetopause. *Journal of Geophysical Research*, *113*(A5), A05218. https://doi.org/10.1029/2007JA012890

Claudepierre, S. G., Mann, I. R., Takahashi, K., Fennell, J. F., Hudson, M. K., Blake, J. B., et al. (2013). Van Allen Probes observation of localized drift resonance between poloidal mode ultra-low frequency waves and 60 keV electrons. *Geophysical Research Letters*, *40*(17), 4491–4497. https://doi.org/10.1002/grl.50901

Constantinescu, O. D., Glassmeier, K.-H., Plaschke, F., Auster, U., Angelopoulos, V., Baumjohann, W., et al. (2009). THEMIS observations of duskside compressional Pc5 waves. *Journal of Geophysical Research*, *114*(A1), A00C25. https://doi.org/10.1029/2008JA013519

Cooper, M. B., Gerrard, A. J., Lanzerotti, L. J., Soto-Chavez, A. R., Kim, H., Kuzichev, I. V., & Goodwin, L. V. (2021). Mirror instabilities in the inner magnetosphere and their potential for localized ULF wave generation. *Journal of Geophysical Research: Space Physics*, *126*(2), e2020JA028773. https://doi.org/10.1029/2020JA028773

Dai, L., Takahashi, K., Wygant, J. R., Chen, L., Bonnell, J., Cattell, C. A., et al. (2013). Excitation of poloidal standing Alfvén waves through drift resonance wave-particle interaction. *Geophysical Research Letters*, *40*(16), 4127–4132. https://doi.org/10.1002/grl.50800

21699402, 2026, 8, Downloaded from https://agupubs.onlinelibrary.wiley.com/doi/10.1029/2025JA035007 by Imperial College London, Wiley Online Library on [03/08/2026]. See the Terms and Conditions (https://onlinelibrary.wiley.com/terms-and-conditions) on Wiley Online Library for rules of use; OA articles are governed by the applicable Creative Commons License

Elkington, S. R., Hudson, M. K., & Chan, A. A. (2003). Resonant acceleration and diffusion of outer zone electrons in an asymmetric geomagnetic field. *Journal of Geophysical Research*, *108*(A3), 1116. https://doi.org/10.1029/2001JA009202

Elkington, S. R., Hudson, M. K., & Chan, A. A. (1999). Acceleration of relativistic electrons via drift-resonant interaction with toroidal-mode Pc-5 ULF oscillations. *Geophysical Research Letters*, *26*(21), 3273–3276. https://doi.org/10.1029/1999GL003659

Elsden, T. (2025). Ultra low frequency waves of Earth's magnetosphere. In *Oxford research encyclopedia of planetary science*. https://doi.org/10.1093/acrefore/9780190647926.013.271

Elsden, T., & Wright, A. N. (2019). The effect of fast normal mode structure and magnetopause forcing on FLRs in a 3-D waveguide. *Journal of Geophysical Research: Space Physics*, *124*(1), 178–196. https://doi.org/10.1029/2018JA026222

Eriksson, P. T. I., Blomberg, L. G., Schaefer, S., & Glassmeier, K.-H. (2006). On the excitation of ULF waves by solar wind pressure enhancements. *Annales Geophysicae*, *24*(11), 3161–3172. https://doi.org/10.5194/angeo-24-3161-2006

Fairfield, D. H. (1971). Average and unusual locations of the Earth's magnetopause and bow shock. *Journal of Geophysical Research (1896-1977)*, *76*(28), 6700–6716. https://doi.org/10.1029/JA076i028p06700

Fairfield, D. H., Baumjohann, W., Paschmann, G., Luhr, H., & Sibeck, D. G. (1990). Upstream pressure variations associated with the bow shock and their effects on the magnetosphere. *Journal of Geophysical Research*, *95*(A4), 3773–3786. https://doi.org/10.1029/JA095iA04p03773

Farrugia, C. J., Gratton, F. T., Bender, L., Biernat, H. K., Erkaev, N. V., Quinn, J. M., et al. (1998). Charts of joint Kelvin-Helmholtz and Rayleigh-Taylor instabilites at the dayside magnetopause for strongly northward interplanetary magnetic field. *Journal of Geophysical Research*, *103*(A4), 6703–6727. https://doi.org/10.1029/97JA03248

Gary, S. P., Fuselier, S. A., & Anderson, B. J. (1993). Ion anisotropy instabilities in the magnetosheath. *Journal of Geophysical Research*, *98*(A2), 1481–1488. https://doi.org/10.1029/92JA01844

Ge, Y. S., McFadden, J. P., Raeder, J., Angelopoulos, V., Larson, D., & Constantinescu, O. D. (2011). Case studies of mirror-mode structures observed by THEMIS in the near-Earth tail during substorms. *Journal of Geophysical Research*, *116*(A1), A01209. https://doi.org/10.1029/2010JA015546

Gillis, E. J., Rijnbeek, R., Kling, R., Speiser, T. W., & Fritz, T. A. (1987). Do flux transfer events cause long-period micropulsations in the dayside magnetosphere? *Journal of Geophysical Research*, *92*(A6), 5820–5826. https://doi.org/10.1029/JA092iA06p05820

Gjerloev, J. W. (2012). The SuperMAG data processing technique. *Journal of Geophysical Research*, *117*(A9), A09213. https://doi.org/10.1029/2012JA017683

Glasmeier, K., Lester, M., Mier-Jedrzejowicz, W. A. C., Green, C. A., Rostoker, G., Orr, D., et al. (1984). Pc5 pulsations and their possible source mechanisms: A case study. *Journal of Geophysics*, *55*(1), 108–119.

GOES N Series Data Book. (2010). GOES N series data book.

Hao, Y. X., Zong, Q.-G., Wang, Y. F., Zhou, X.-Z., Zhang, H., Fu, S. Y., et al. (2014). Interactions of energetic electrons with ULF waves triggered by interplanetary shock: Van Allen Probes observations in the magnetotail. *Journal of Geophysical Research: Space Physics*, *119*(10), 8262–8273. https://doi.org/10.1002/2014JA020023

Hartinger, M., Angelopoulos, V., Moldwin, M. B., Nishimura, Y., Turner, D. L., Glassmeier, K.-H., et al. (2012). Observations of a Pc5 global (cavity/waveguide) mode outside the plasmasphere by THEMIS. *Journal of Geophysical Research*, *117*(A6), A06202. https://doi.org/10.1029/2011JA017266

Hartinger, M., Angelopoulos, V., Moldwin, M. B., Takahashi, K., & Clausen, L. B. N. (2013). Statistical study of global modes outside the plasmasphere. *Journal of Geophysical Research: Space Physics*, *118*(2), 804–822. https://doi.org/10.1002/jgra.50140

Hartinger, M., Elsden, T., Archer, M. O., Takahashi, K., Wright, A. N., Artemyev, A., et al. (2023). Properties of magnetohydrodynamic normal modes in the Earth's magnetosphere. *Journal of Geophysical Research: Space Physics*, *128*(12), e2023JA031987. https://doi.org/10.1029/2023JA031987

Hartinger, M., Plaschke, F., Archer, M. O., Welling, D. T., Moldwin, M. B., & Ridley, A. (2015). The global structure and time evolution of dayside magnetopause surface eigenmodes. *Geophysical Research Letters*, *42*(8), 2594–2602. https://doi.org/10.1002/2015GL063623

Hartinger, M., Turner, D. L., Plaschke, F., Angelopoulos, V., & Singer, H. (2013). The role of transient ion foreshock phenomena in driving Pc5 ULF wave activity. *Journal of Geophysical Research: Space Physics*, *118*(1), 299–312. https://doi.org/10.1029/2012JA018349

Hasegawa, A. (1969). Drift mirror instability in the magnetosphere. *The Physics of Fluids*, *12*(12), 2642–2650. https://doi.org/10.1063/1.1692407

Hughes, W. J. (1994). Magnetospheric ULF waves: A tutorial with a historical perspective. In *Solar wind sources of magnetospheric ultra-low-frequency waves* (pp. 1–11). American Geophysical Union (AGU). https://doi.org/10.1029/GM081p0001

Hughes, W. J., & Southwood, D. J. (1976). The screening of micropulsation signals by the atmosphere and ionosphere. *Journal of Geophysical Research (1896-1977)*, *81*(19), 3234–3240. https://doi.org/10.1029/JA081i019p03234

Hughes, W. J., Southwood, D. J., Mauk, B., Mcpherron, R. L., & Barfield, J. N. (1978). Alfvén waves generated by an inverted plasma energy distribution. *Nature*, *275*(5675), 43–45. https://doi.org/10.1038/275043a0

Hwang, K.-J., & Sibeck, D. G. (2016). Role of low-frequency boundary waves in the dynamics of the dayside magnetopause and the inner magnetosphere. In *Low-Frequency waves in space plasmas* (pp. 213–239). American Geophysical Union (AGU). https://doi.org/10.1002/9781119055006.ch13

Jacobs, J. A., Kato, Y., Matsushita, S., & Troitskaya, V. A. (1964). Classification of geomagnetic micropulsations. *Journal of Geophysical Research (1896-1977)*, *69*(1), 180–181. https://doi.org/10.1029/JZ069i001p00180

Kavosi, S., & Raeder, J. (2015). Ubiquity of Kelvin–Helmholtz waves at Earth's magnetopause. *Nature Communications*, *6*(1), 7019. https://doi.org/10.1038/ncomms8019

Kepko, L., & Spence, H. E. (2003). Observations of discrete, global magnetospheric oscillations directly driven by solar wind density variations. *Journal of Geophysical Research*, *108*(A6), 1257. https://doi.org/10.1029/2002JA009676

Kepko, L., Spence, H. E., & Singer, H. J. (2002). ULF waves in the solar wind as direct drivers of magnetospheric pulsations. *Geophysical Research Letters*, *29*(8), 39-1–4. https://doi.org/10.1029/2001GL014405

Kivelson, M. G., Cao, M., Mcpherron, R. L., & Walker, R. J. (1997). A possible signature of magnetic cavity mode oscillations in ISEE spacecraft observations. *Journal of Geomagnetism and Geoelectricity*, *49*(9), 1079–1098. https://doi.org/10.5636/jgg.49.1079

Kivelson, M. G., & Southwood, D. J. (1985). Resonant ULF waves: A new interpretation. *Geophysical Research Letters*, *12*(1), 49–52. https://doi.org/10.1029/GL012i001p00049

Kivelson, M. G., & Southwood, D. J. (1986). Coupling of global magnetospheric MHD eigenmodes to field line resonances. *Journal of Geophysical Research*, *91*(A4), 4345–4351. https://doi.org/10.1029/JA091iA04p04345

Korotova, G. I., Sibeck, D., Engebretson, M., Balikhin, M., Thaller, S., Kletzing, C., et al. (2020). Multipoint observations of compressional Pc5 pulsations in the dayside magnetosphere and corresponding particle signatures. *Annales Geophysicae*, *38*(6), 1267–1281. https://doi.org/10.5194/angeo-38-1267-2020

Korotova, G. I., & Sibeck, D. G. (2024). Multipoint observations of compressional Pc5-6 pulsations in the dawn side magnetosphere: A case study. *Advances in Space Research*, *73*(1), 597–606. https://doi.org/10.1016/j.asr.2023.10.018

Kuo, H., Russell, C. T., & Le, G. (1995). Statistical studies of flux transfer events. *Journal of Geophysical Research*, *100*(A3), 3513–3519. https://doi.org/10.1029/94JA02498

Lacombe, C., & Belmont, G. (1995). Waves in the Earth's magnetosheath: Observations and interpretations. *Advances in Space Research*, *15*(8), 329–340. https://doi.org/10.1016/0273-1177(94)00113-F

Lanzerotti, L. J. (1988). Comment on "Do flux transfer events cause long-period micropulsations in the dayside magnetosphere?" by Gillis et al. *Journal of Geophysical Research*, *93*(A4), 2763–2764. https://doi.org/10.1029/JA093iA04p02763

Lazzeri, C., Samsonov, A., Forsyth, C., Branduardi-Raymont, G., & Bogdanova, Y. V. (2024). A statistical Study of the properties of, and geomagnetic responses to, large, rapid southward turnings of the interplanetary magnetic field. *Journal of Geophysical Research: Space Physics*, *129*(9), e2023JA032160. https://doi.org/10.1029/2023JA032160

Le, G., Chen, S.-H., Zheng, Y., Russell, C. T., Slavin, J. A., Huang, C., et al. (2004). Coordinated polar spacecraft, geosynchronous spacecraft, and ground-based observations of magnetopause processes and their coupling to the ionosphere. *Annales Geophysicae*, *22*(12), 4329–4350. https://doi.org/10.5194/angeo-22-4329-2004

Liu, J., Angelopoulos, V., Sibeck, D., Phan, T., Pu, Z. Y., McFadden, J., et al. (2008). THEMIS observations of the dayside traveling compression region and flows surrounding flux transfer events. *Geophysical Research Letters*, *35*(17), L17S07. https://doi.org/10.1029/2008GL033673

Mager, O. V., Chelpanov, M. A., Mager, P. N., Klimushkin, D. Y., & Berngardt, O. I. (2019). Conjugate ionosphere-magnetosphere observations of a sub-alfvénic compressional Intermediate-m wave: A case Study using EKB radar and Van Allen probes. *Journal of Geophysical Research: Space Physics*, *124*(5), 3276–3290. https://doi.org/10.1029/2019JA026541

Mann, I. R., Murphy, K. R., Ozeke, L. G., Rae, I. J., Milling, D. K., Kale, A. A., & Honary, F. F. (2012). The role of ultralow frequency waves in radiation Belt dynamics. In *Dynamics of the Earth's radiation belts and inner magnetosphere* (pp. 69–92). American Geophysical Union (AGU). https://doi.org/10.1029/2012GM001349

Mann, I. R., Voronkov, I., Dunlop, M., Donovan, E., Yeoman, T. K., Milling, D. K., et al. (2002). Coordinated ground-based and Cluster observations of large amplitude global magnetospheric oscillations during a fast solar wind speed interval. *Annales Geophysicae*, *20*(4), 405–426. https://doi.org/10.5194/angeo-20-405-2002

Mann, I. R., Wright, A. N., Mills, K. J., & Nakariakov, V. M. (1999). Excitation of magnetospheric waveguide modes by magnetosheath flows. *Journal of Geophysical Research*, *104*(A1), 333–353. https://doi.org/10.1029/1998JA900026

McFadden, J. P., Carlson, C. W., Larson, D., Ludlam, M., Abiad, R., Elliott, B., et al. (2008). The THEMIS ESA plasma instrument and In-flight calibration. *Space Science Reviews*, *141*(1), 277–302. https://doi.org/10.1007/s11214-008-9440-2

Michael, C. M., Yeoman, T. K., Wright, D. M., Chelpanov, M. A., & Mager, P. N. (2024). Evolving phase propagation in an Intermediate-m ULF wave driven by substorm-injected particles. *Journal of Geophysical Research: Space Physics*, *129*(3), e2023JA031654. https://doi.org/10.1029/2023JA031654

Murphy, K. R., Inglis, A. R., Sibeck, D. G., Rae, I. J., Watt, C. E. J., Silveira, M., et al. (2018). Determining the mode, frequency, and azimuthal wave number of ULF waves during a HSS and moderate geomagnetic storm. *Journal of Geophysical Research: Space Physics*, *123*(8), 6457–6477. https://doi.org/10.1029/2017JA024877

Murphy, K. R., Mann, I. R., & Sibeck, D. G. (2015). On the dependence of storm time ULF wave power on magnetopause location: Impacts for ULF wave radial diffusion. *Geophysical Research Letters*, *42*(22), 9676–9684. https://doi.org/10.1002/2015GL066592

Nagano, H., & Araki, T. (1983). Long-duration Pc5 pulsations observed by geostationary satellites. *Geophysical Research Letters*, *10*(9), 908–911. https://doi.org/10.1029/GL010i009p00908

Olson, J. V., & Rostoker, G. (1978). Longitudinal phase variations of Pc 4-5 micropulsations. *Journal of Geophysical Research*, *83*(A6), 2481–2488. https://doi.org/10.1029/JA083iA06p02481

Ozeke, L. G., & Mann, I. R. (2008). Energization of radiation belt electrons by ring current ion driven ULF waves. *Journal of Geophysical Research*, *113*(A2), A02201. https://doi.org/10.1029/2007JA012468

Paschmann, G., & Daly, P. W. (1998). *Analysis methods for multi-spacecraft data*. International Space Science Institute.

Paschmann, G., Haerendel, G., Papamastorakis, I., Sckopke, N., Bame, S. J., Gosling, J. T., & Russell, C. T. (1982). Plasma and magnetic field characteristics of magnetic flux transfer events. *Journal of Geophysical Research*, *87*(A4), 2159–2168. https://doi.org/10.1029/JA087iA04p02159

Plaschke, F., & Glassmeier, K.-H. (2011). Properties of standing kruskal-schwarzschild-modes at the magnetopause. *Annales Geophysicae*, *29*(10), 1793–1807. https://doi.org/10.5194/angeo-29-1793-2011

Plaschke, F., Hietala, H., & Angelopoulos, V. (2013). Anti-sunward high-speed jets in the subsolar magnetosheath. *Annales Geophysicae*, *31*(10), 1877–1889. https://doi.org/10.5194/angeo-31-1877-2013

Pokhotelov, O. A., Pilipenko, V. A., & Amata, E. (1985). Drift anisotropy instability of a finite-β magnetospheric plasma. *Planetary and Space Science*, *33*(11), 1229–1241. https://doi.org/10.1016/0032-0633(85)90001-7

Prikryl, P., Greenwald, R. A., Sofko, G. J., Villain, J. P., Ziesolleck, C. W. S., & Friis-Christensen, E. (1998). Solar-wind-driven pulsed magnetic reconnection at the dayside magnetopause, Pc5 compressional oscillations, and field line resonances. *Journal of Geophysical Research*, *103*(A8), 17307–17322. https://doi.org/10.1029/97JA03595

Rae, I. J., Donovan, E. F., Mann, I. R., Fenrich, F. R., Watt, C. E. J., Milling, D. K., et al. (2005). Evolution and characteristics of global Pc5 ULF waves during a high solar wind speed interval. *Journal of Geophysical Research*, *110*(A12), A12211. https://doi.org/10.1029/2005JA011007

Rae, I. J., Mann, I. R., Watt, C. E. J., Kistler, L. M., & Baumjohann, W. (2007). Equator-S observations of drift mirror mode waves in the dawnside magnetosphere. *Journal of Geophysical Research*, *112*(A11), A11203. https://doi.org/10.1029/2006JA012064

Rae, I. J., Watt, C. E. J., Fenrich, F. R., Mann, I. R., Ozeke, L. G., & Kale, A. (2007). Energy deposition in the ionosphere through a global field line resonance. *Annales Geophysicae*, *25*(12), 2529–2539. https://doi.org/10.5194/angeo-25-2529-2007

Richardson, I., & Cane, H. (2024). Near-Earth interplanetary coronal mass ejections since January 1996. *Harvard Dataverse*. https://doi.org/10.7910/DVN/C2MHTH

Rijnbeek, R. P., Cowley, S. W. H., Southwood, D. J., & Russell, C. T. (1984). A survey of dayside flux transfer events observed by ISEE 1 and 2 magnetometers. *Journal of Geophysical Research*, *89*(A2), 786–800. https://doi.org/10.1029/JA089iA02p00786

Russell, C. T., & Elphic, R. C. (1978). Initial ISEE magnetometer results: Magnetopause observations. *Space Science Reviews*, *22*(6), 681–715. https://doi.org/10.1007/BF00212619

Samson, J. C., Harrold, B. G., Ruohoniemi, J. M., Greenwald, R. A., & Walker, A. D. M. (1992). Field line resonances associated with MHD waveguides in the magnetosphere. *Geophysical Research Letters*, *19*(5), 441–444. https://doi.org/10.1029/92GL00116

21699402, 2026, 8, Downloaded from https://agupubs.onlinelibrary.wiley.com/doi/10.1029/2025JA035007 by Imperial College London, Wiley Online Library on [03/08/2026]. See the Terms and Conditions (https://onlinelibrary.wiley.com/terms-and-conditions) on Wiley Online Library for rules of use; OA articles are governed by the applicable Creative Commons License

21699402, 2026, 8, Downloaded from https://agupubs.onlinelibrary.wiley.com/doi/10.1029/2025JA035007 by Imperial College London, Wiley Online Library on [03/08/2026]. See the Terms and Conditions (https://onlinelibrary.wiley.com/terms-and-conditions) on Wiley Online Library for rules of use; OA articles are governed by the applicable Creative Commons License

Samsonov, A. A., Sibeck, D. G., Dmitrieva, N. P., Semenov, V. S., Slivka, K. Y., Šafránkova, J., & Němeček, Z. (2018). Magnetosheath propagation time of solar wind directional discontinuities. *Journal of Geophysical Research: Space Physics*, *123*(5), 3727–3741. https://doi.org/10.1029/2017JA025174

Samsonov, A. A., Sibeck, D. G., Zolotova, N. V., Biernat, H. K., Chen, S.-H., Rastaetter, L., et al. (2011). Propagation of a sudden impulse through the magnetosphere initiating magnetospheric Pc5 pulsations. *Journal of Geophysical Research*, *116*(A10), A10216. https://doi.org/10.1029/2011JA016706

Sen, A. K. (1965). Stability of the magnetospheric boundary. *Planetary and Space Science*, *13*(2), 131–141. https://doi.org/10.1016/0032-0633(65)90182-0

Shue, J.-H., Song, P., Russell, C. T., Steinberg, J. T., Chao, J. K., Zastenker, G., et al. (1998). Magnetopause location under extreme solar wind conditions. *Journal of Geophysical Research*, *103*(A8), 17691–17700. https://doi.org/10.1029/98JA01103

Sibeck, D. G. (2004). Pressure pulses and cavity mode resonances. In J.-A. Sauvaud & Z. Němeček (Eds.), *Multiscale processes in the Earth's magnetosphere: From interball to cluster* (pp. 95–110). Springer Netherlands. https://doi.org/10.1007/1-4020-2768-0_6

Singer, H. J., Southwood, D. J., Walker, R. J., & Kivelson, M. G. (1981). Alfven wave resonances in a realistic magnetospheric magnetic field geometry. *Journal of Geophysical Research*, *86*(A6), 4589–4596. https://doi.org/10.1029/JA086iA06p04589

Song, P., Elphic, R. C., & Russell, C. T. (1988). ISEE 1 and 2 observations of the oscillating magnetopause. *Geophysical Research Letters*, *15*(8), 744–747. https://doi.org/10.1029/GL015i008p00744

Sonnerup, B. U. O., & Cahill, L. J., Jr. (1967). Magnetopause structure and attitude from Explorer 12 observations. *Journal of Geophysical Research (1896-1977)*, *72*(1), 171–183. https://doi.org/10.1029/JZ072i001p00171

Soto-Chavez, A. R., Lanzerotti, L. J., Manweiler, J. W., Gerrard, A., Cohen, R., Xia, Z., & Kim, H. (2019). Observational evidence of the drift-mirror plasma instability in Earth's inner magnetosphere | Physics of Plasmas. *AIP Publishing. Physics of Plasmas*, *206*, 042110. https://doi.org/10.1063/1.5083629

Southwood, D. J. (1974). Some features of field line resonances in the magnetosphere. *Planetary and Space Science*, *22*(3), 483–491. https://doi.org/10.1016/0032-0633(74)90078-6

Southwood, D. J., Dungey, J. W., & Etherington, R. J. (1969). Bounce resonant interaction between pulsations and trapped particles. *Planetary and Space Science*, *17*(3), 349–361. https://doi.org/10.1016/0032-0633(69)90068-3

Southwood, D. J., & Kivelson, M. G. (1981). Charged particle behavior in low-frequency geomagnetic pulsations 1. Transverse waves. *Journal of Geophysical Research*, *86*(A7), 5643–5655. https://doi.org/10.1029/JA086iA07p05643

Southwood, D. J., & Kivelson, M. G. (1982). Charged particle behavior in low-frequency geomagnetic pulsations, 2. Graphical approach. *Journal of Geophysical Research*, *87*(A3), 1707–1710. https://doi.org/10.1029/JA087iA03p01707

Stephenson, J. a. E., & Walker, A. D. M. (2002). HF radar observations of Pc5 ULF pulsations driven by the solar wind. *Geophysical Research Letters*, *29*(9), 8-1–4. https://doi.org/10.1029/2001GL014291

Takahashi, K., Elsden, T., Wright, A. N., & Degeling, A. W. (2023). Polarization of magnetospheric ULF waves excited by an interplanetary shock on 27 February 2014. *Journal of Geophysical Research: Space Physics*, *128*(9), e2023JA031608. https://doi.org/10.1029/2023JA031608

Takahashi, K., Higbie, P. R., & Baker, D. N. (1985). Azimuthal propagation and frequency characteristic of compressional Pc 5 waves observed at geostationary orbit. *Journal of Geophysical Research*, *90*(A2), 1473–1485. https://doi.org/10.1029/JA090iA02p01473

Takahashi, K., Lysak, R., Vellante, M., Kletzing, C. A., Hartinger, M. D., & Smith, C. W. (2018). Observation and Numerical Simulation of cavity mode oscillations excited by an interplanetary shock. *Journal of Geophysical Research: Space Physics*, *123*(3), 1969–1988. https://doi.org/10.1002/2017JA024639

Tóth, G., Sokolov, I. V., Gombosi, T. I., Chesney, D. R., Clauer, C. R., De Zeeuw, D. L., et al. (2005). Space Weather Modeling Framework: A new tool for the space science community. *Journal of Geophysical Research*, *110*(A12), A12226. https://doi.org/10.1029/2005JA011126

Trattner, K. J., Mulcock, J. S., Petrinec, S. M., & Fuselier, S. A. (2007). Probing the boundary between antiparallel and component reconnection during southward interplanetary magnetic field conditions. *Journal of Geophysical Research*, *112*(A8), A08210. https://doi.org/10.1029/2007JA012270

Tsyganenko, N. A., & Sitnov, M. I. (2005). Modeling the dynamics of the inner magnetosphere during strong geomagnetic storms. *Journal of Geophysical Research*, *110*(A3), A03208. https://doi.org/10.1029/2004JA010798

Usanova, M. E., Mann, I. R., Bortnik, J., Shao, L., & Angelopoulos, V. (2012). THEMIS observations of electromagnetic ion cyclotron wave occurrence: Dependence on AE, SYMH, and solar wind dynamic pressure. *Journal of Geophysical Research*, *117*(A10), A10218. https://doi.org/10.1029/2012JA018049

Usanova, M. E., Mann, I. R., Rae, I. J., Kale, Z. C., Angelopoulos, V., Bonnell, J. W., et al. (2008). Multipoint observations of magnetospheric compression-related EMIC Pc1 waves by THEMIS and CARISMA. *Geophysical Research Letters*, *35*(17), L17S25. https://doi.org/10.1029/2008GL034458

Viall, N. M., Kepko, L., & Spence, H. E. (2009). Relative occurrence rates and connection of discrete frequency oscillations in the solar wind density and dayside magnetosphere. *Journal of Geophysical Research*, *114*(A1), A01201. https://doi.org/10.1029/2008JA013334

Wang, B., Liu, T., Nishimura, Y., Zhang, H., Hartinger, M., Shi, X., et al. (2020). Global propagation of magnetospheric Pc5 ULF waves driven by foreshock transients. *Journal of Geophysical Research: Space Physics*, *125*(12), e2020JA028411. https://doi.org/10.1029/2020JA028411

Wang, C., Thorne, R., Liu, T. Z., Hartinger, M. D., Nagai, T., Angelopoulos, V., et al. (2017). A multispacecraft event study of Pc5 ultralow-frequency waves in the magnetosphere and their external drivers. *Journal of Geophysical Research: Space Physics*, *122*(5), 5132–5147. https://doi.org/10.1002/2016JA023610

Waters, C. L., Menk, F. W., & Fraser, B. J. (1991). The resonance structure of low latitude Pc3 geomagnetic pulsations. *Geophysical Research Letters*, *18*(12), 2293–2296. https://doi.org/10.1029/91GL02550

Woch, J., Kremser, G., Korth, A., Pokhotelov, O. A., Pilipenko, V. A., Nezlina, Y. M., & Amata, E. (1988). Curvature-driven drift mirror instability in the magnetosphere. *Planetary and Space Science*, *36*(4), 383–393. https://doi.org/10.1016/0032-0633(88)90126-2

Wright, A. N., & Rickard, G. J. (1995). A numerical Study of resonant absorption in a magnetohydrodynamic cavity driven by a broadband spectrum. *The Astrophysical Journal*, *444*, 458. https://doi.org/10.1086/175620

Xie, Z.-K., Zong, Q. G., Ren, J., Yue, C., Liu, Z.-Y., Liu, J.-J., et al. (2023). Global ULF waves excited by solar wind dynamic pressure impulses: 1. Timescales and geomagnetic activity dependence. *Journal of Geophysical Research: Space Physics*, *128*(10), e2023JA031813. https://doi.org/10.1029/2023JA031813

Yang, B., Zong, Q.-G., Wang, Y. F., Fu, S. Y., Song, P., Fu, H. S., et al. (2010). Cluster observations of simultaneous resonant interactions of ULF waves with energetic electrons and thermal ion species in the inner magnetosphere. *Journal of Geophysical Research*, *115*(A2), A02214. https://doi.org/10.1029/2009JA014542

Yeoman, T. K., Klimushkin, D. Y., & Mager, P. N. (2010). Intermediate-*m* ULF waves generated by substorm injection: A case study. *Annales Geophysicae*, *28*(8), 1499–1509. https://doi.org/10.5194/angeo-28-1499-2010

Zhang, X. Y., Zong, Q.-G., Wang, Y. F., Zhang, H., Xie, L., Fu, S. Y., et al. (2010). ULF waves excited by negative/positive solar wind dynamic pressure impulses at geosynchronous orbit. *Journal of Geophysical Research*, *115*(A10), A10221. https://doi.org/10.1029/2009JA015016

Zong, Q.-G., Zhou, X.-Z., Wang, Y. F., Li, X., Song, P., Baker, D. N., et al. (2009). Energetic electron response to ULF waves induced by interplanetary shocks in the outer radiation belt. *Journal of Geophysical Research*, *114*(A10), A10204. https://doi.org/10.1029/2009JA014393

21699402, 2026, 8, Downloaded from https://agupubs.onlinelibrary.wiley.com/doi/10.1029/2025JA035007 by Imperial College London, Wiley Online Library on [03/08/2026]. See the Terms and Conditions (https://onlinelibrary.wiley.com/terms-and-conditions) on Wiley Online Library for rules of use; OA articles are governed by the applicable Creative Commons License